Effects of charge carrier behavior on device performance of organic solar cells

SHINTAKU NAOTO

Doctor of Philosophy

Department of Functional Molecular Science
School of Physical Sciences
SOKENDAI (The Graduate University for Advanced Studies)

Effects of charge carrier behavior on device performance of organic solar cells

Naoto Shintaku

SOKENDAI (The Graduate University for Advanced Studies)

School of Physical Sciences

Dept. of Functional Molecular Science

Contents

Chapter 1:

General Introduction

1.1. Background of organic solar cells

A single layer organic solar cell (OSC) in which an organic layer is sandwiched between two different metals (Fig. 1.1.1. (a)) had a photo-conversion efficiency (PCE) of 0.1% range due to the inefficient exciton dissociation[1–3]. In 1986, Tang et al. reported on planar hetero junction (PHJ) OSCs using electron donors (D) and electron acceptors (A)[4]. The donor layer was deposited on a transparent electrode, and the acceptor layer was deposited on the donor layer (Fig. 1.1.1. (b)). Efficient exciton dissociation at the interface between the donor and acceptor layers was obtained. However, the exciton diffusion length in the organic layers was short[5], inhibiting charge generation. To generate a large amount of charge, a *pin* structure was introduced (Fig. 1.1.1. (c)) [6,7]. The *i* layer was fabricated by a co-deposition technique. Exciton dissociation occurred in the whole region due to the mixed structure of donors and acceptors. As a result, high photo-current densities were obtained in OSCs with an *i* layer. The *i* layer has been applied to polymer OSCs, namely, bulk hetero junctions (BHJ) (Fig. 1.1.1. (d)) [8,9]. BHJ OSCs with PCEs of the order of 10% have been developed using optimized polymer material[10–12]. Recently, flexible, wearable and mobile devices based on BHJ OSCs have been fabricated[13–16]. These unique devices are attracting considerable attention as next generation battery and energy devices.

Efficiency of OSCs has been improved by efficient charge generation and transport. The charge generation was increased in co-deposited films, and the efficient charge transport was realized by the crystalline organic materials. The efficient charge generation and transport increased short-circuit photocurrent (J_{SC}) [17]. The J_{SC} in OSCs is already enough large. On the other hands, observed open-circuit voltage (V_{OC}) is lower than the expected value. This V_{OC} loss remains an issue for the PCE of OSCs. Previously, the increase in the V_{OC} has been realized using various combinations of donor and acceptor materials. However, each combination still had the large V_{OC} loss about 0.5 V due to charge recombinations [18,19]. Following these considerations, the author attempts to clarify the relationships between the V_{OC} and the charge carrier behavior in the OSCs.

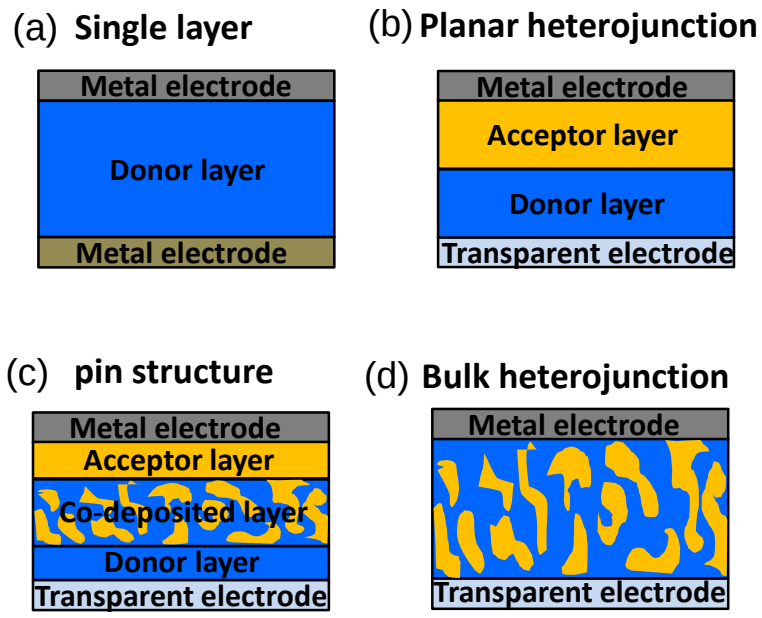

Fig. 1.1.1. Schematic illustrations of organic solar cells (a) single layer, (b) planar heterojunction, (c) *pin* structure and (d) bulk heterojunction.

1.2. Photo-conversion process in organic solar cells

The photo-conversion process in an organic solar cell is shown in Fig. 1.2.1. After the OSCs absorb light, excitons are generated. The exciton is localized at a molecule, and the excited electron and hole are bound together by Coulomb attraction[20]. This Frenkel type exciton cannot be separated by the thermal energy. In contrast, excitons in inorganic semiconductors can be separated by the thermal energy due to the high permittivity. The generated excitons diffuse through the organic layer, but the diffusion length is short[5]. If the excitons reach the donor/acceptor interface before decaying, the electrons are transferred to the lowest unoccupied molecular orbital (LUMO) of the acceptor molecule, or the holes are transferred to the highest occupied molecular orbital (HOMO) of the donor molecule. The separated charge is stabilized by the Coulomb energy[21]. This state is called the charge transfer (CT) state.

When the charge escapes from the CT state, free holes and electrons are generated. The free holes and electrons are transported through the donor and acceptor regions, respectively. These charge carriers are transported by the potential difference as drift current or by the charge concentration difference as diffusion current. The charge transport is described as hopping conduction, as they are transported from molecule to molecule. The holes and electrons recombine at the donor/acceptor interface. This charge recombination process causes a loss of photo-current in the OSCs.

The charge carriers are collected at the electrodes. In order to collect them it is important that the energy barrier at the organic semiconductor/electrode interface is as small as possible. When there is no energy barrier at the interface, the contact is ohmic. To make ohmic contact sufficiently, high or low work function materials are inserted at the semiconductor/electrode interface.

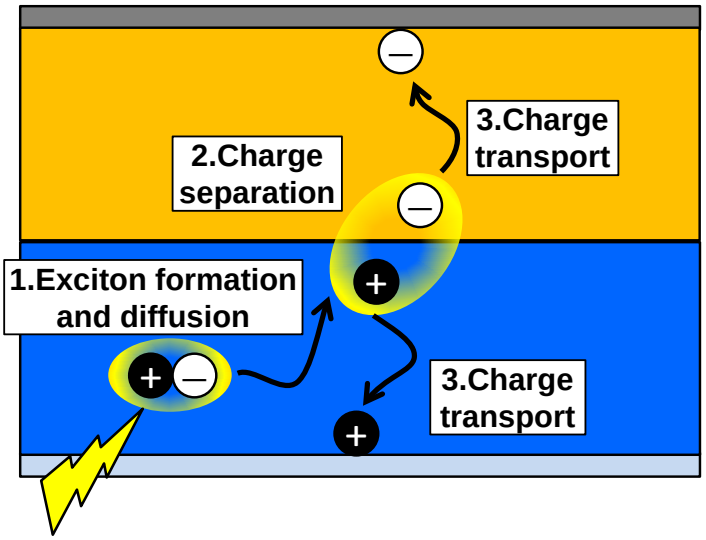

Fig. 1.2.1. Schematic illustration of the photo-conversion process in an organic solar cell.

1.3. Behavior of charge carriers in organic solar cells

The photo-conversion process in an OSC and the performance of an OSC depends strongly on the charge carrier behavior. In this section, the relevant features of this behavior are described.

1.3.1. Charge carrier transport

Hopping conduction

The conduction mechanism in organic semiconductor is hopping conduction, where charged particles are transported from molecule to molecule[22,23]. In other words, the charge in a localized state is repeatedly transported to the next localized state (Fig 1.3.1.). Hopping conduction is dominated by releasing and trapping processes at these states. The charge carrier mobility in organic semiconductors is lower than in inorganic semiconductors. Such low carrier mobility limits the current in organic devices. This current is a space charge limited current (SCLC), and is given by the following equation[24]:

$$J_{SCLC} = \frac{9}{8}\varepsilon\mu\frac{V^2}{d^3}$$

where J_{SCLC} is the current density, ε is the permittivity of the material, μ is the carrier mobility, V is the voltage and d is the thickness of the layer. The SCLC can be found from the slope of the *J*-*V* characteristics. At low voltage, the characteristics are ohmic with a slope of 1. On increasing the voltage, the current is limited to the organic region and the slope changes to 2. When there are deep traps, the slope is further increased to over 2[25].

The charge transport process, that is, the repeated releasing and trapping at localized traps, can be represented by a multiple trapping model (MTM)[26–28]. A

schematic illustration of the MTM is shown in fig. 1.3.1. The charge carriers can be released from shallow traps by thermal energy. However, charge carriers captured at deep traps cannot be released by the thermal energy. The time for which the charge carrier is captured at a deep trap is the deep trapping lifetime (τ). τ is a parameter that can be used to determine the range of the charge carriers (L), which is the average distance that the injected carriers can move until they are captured by the deep traps. The relationship between L and τ is as follows[29]:

$$L = \mu\tau E$$

If L is greater than the thickness of the active layer, the charge transport is sufficient for the OSC.

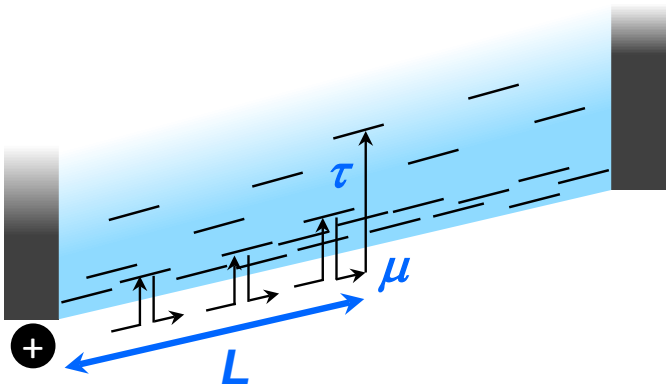

Fig. 1.3.1. Schematic illustration of the multiple trapping model.

Measurement (Impedance spectroscopy)

Some measurement methods have been developed and applied to obtain the charge transport parameters. According to previous reports, the charge carrier behavior is related to the capacitance-frequency (*C-f*) curve[30,31]. μ and τ can be obtained simultaneously from the *C-f* curves. A useful technique to obtain *C-f* curves, is to make impedance spectroscopy (IS) measurements.

To make IS measurements an AC voltage is applied to the device and the AC current is measured. The impedance ($|Z|$) is calculated using the absolute values of the AC voltage and current. The phase (θ_Z) of the impedance is equal to the difference in phase between the input voltage and output current. The equivalent circuit for electron or hole only transport devices is a resistor and a capacitor in parallel, the admittance of which is given by the following equation[32]:

$$|Y| = G + j\omega C, \ |Y| = 1/|Z|$$

where Y is the admittance, G is the conductance, ω is the angular frequency, and C is the capacitance. The capacitance can be obtained from the IS measurements using the following relationship:

$$\omega C = |Y| \sin(-\theta_Z)$$

To obtain μ and τ using impedance spectroscopy, hole-only or electron-only devices are needed. In addition, a DC voltage is applied to the device with the AC voltage to make SCLC condition.

1.3.2. Charge carrier recombination

Recombination occurs when free holes and electrons approach each other[33]. The electron and hole are bound by Coulomb attraction soon after exciton dissociation. The electron-hole pair decays to the ground state, a process known as geminate recombination. When a free hole and free electron meet and recombine at the donor/acceptor interface, these charge carriers decay to the ground state via bimolecular recombination (Fig. 1.3.2, left).

Bimolecular recombination is defined as direct Langevin recombination. This bimolecular recombination has been applied to crystalline inorganic semiconductors. However, the disorder in organic semiconductors is not negligible. The disorder in an organic semiconductor results in trapped charge at the localized states. This trapped charge and free charge of the opposite polarity meet and decay to the ground state via trap-assisted recombination (Fig. 1.3.2, right) [34,35].

Since efficient exciton dissociation has been realized at a donor/acceptor interface, the effect of non-geminate recombination on the performance of OSCs is a significant problem.

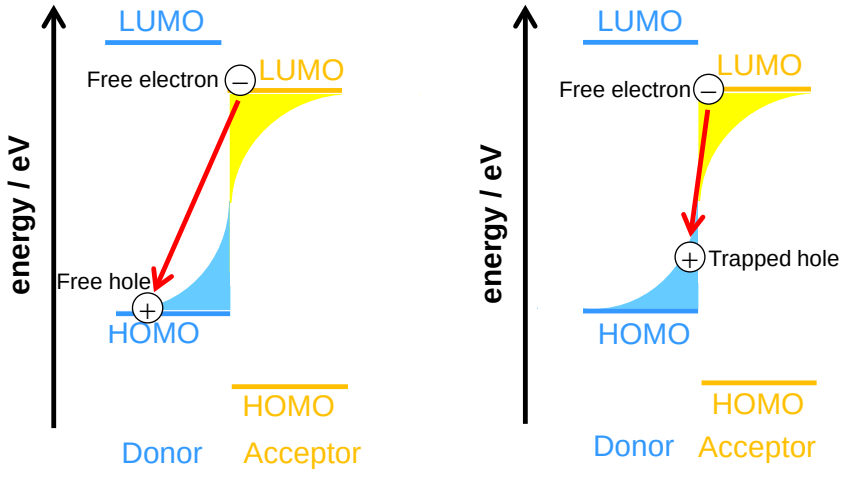

Fig. 1.3.2. Schematic illustration of the charge recombination process.

1.3.3. Impurity doping

Impurity doping is a basic technique in the field of semiconductor devices[36,37]. If an acceptor dopant is introduced into an organic semiconductor, electron transfer from the semiconductor to the dopant occurs (Fig. 1.3.3). As a result, the organic molecule becomes an anion species, and a hole is generated. Moreover, the acceptor dopant causes an increase in the work function of the organic semiconductor (Fig. 1.3.4). In contrast, an organic semiconductor with a donor type dopant decreases the work function because electron transfer from the dopant to the organic molecule occurs.

The amount the work function changes depends on the concentration of the dopant in the organic semiconductor (Fig.1.3.4). Thus, the work function of the semiconductor can be controlled by the impurity doping. In addition, the impurity doping increases the conductance of the semiconductor because the charge carrier density is increased[38]. Moreover, the trap states are filled by the induced charge. This trap filling effect causes an increase in the performance of BHJ OSCs[39,40].

Dopant in a small organic semiconductor layer is introduced by co-deposition. The dopant concentration is controlled by the ratio of the deposition rates. Recently, a deposition rate of the dopant has been decreased using a rotating shutter, and 1 ppm dopant concentration has been realized[41].

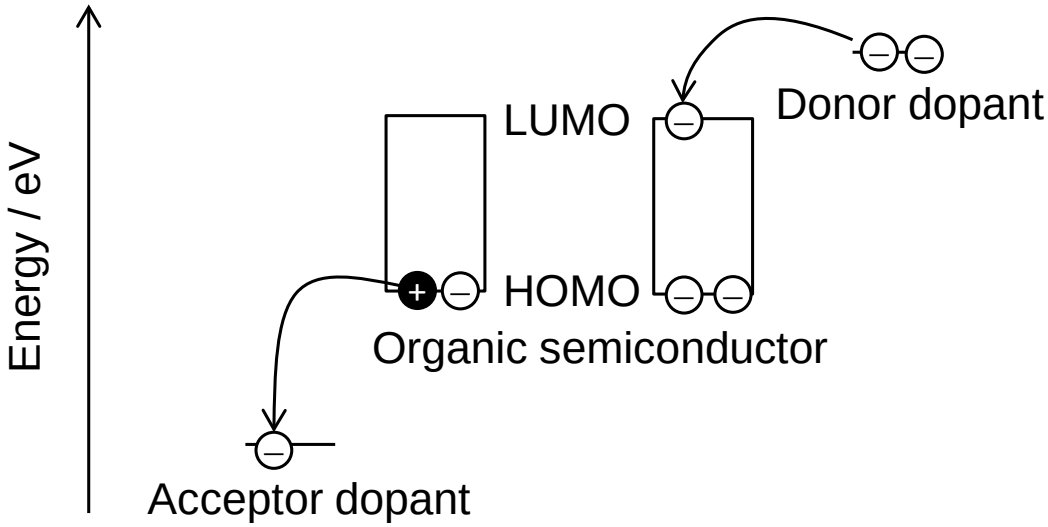

Fig. 1.3.3. Energy band diagram of an organic semiconductor with dopant.

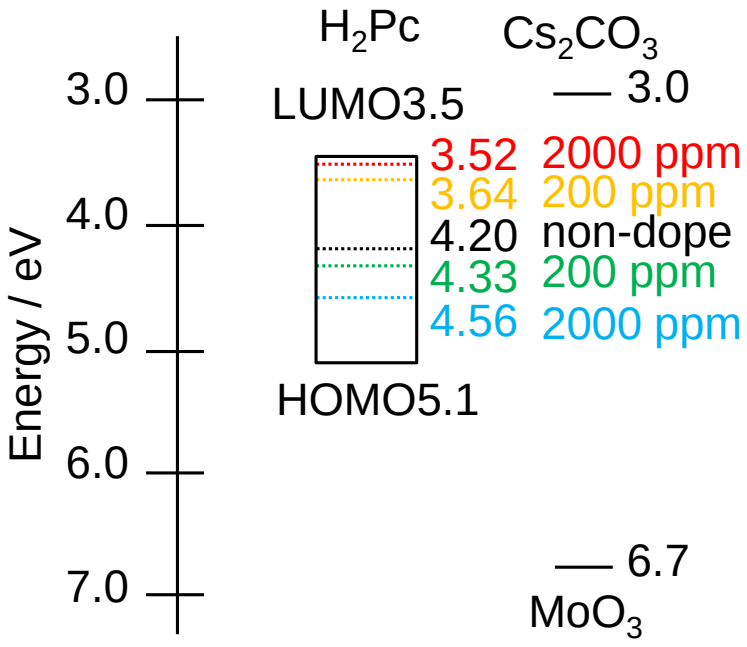

Fig. 1.3.4. Energy levels of H_2Pc. The dashed lines indicate the work functions of a 50 nm thick H_2Pc layer with no dopant (black), doped with 200 ppm MoO_3 (green), doped with 2000 ppm MoO_3 (blue), doped with 200 ppm Cs_2CO_3 (orange), and doped with 2000 ppm Cs_2CO_3 (red) on ITO substrates.

1.3.4. Energy level alignment

The alignment of the energy levels at the organic semiconductor/electrode and the organic semiconductor/organic semiconductor interface is important for the performance of the OSCs[42–44]. If the work function of the electrode (W_m) is greater than the HOMO level of the donor molecule (Fig. 1.3.5. (a)), electron diffusion from the donor molecule to the electrode occurs after contact. The Fermi energy (E_F) is pinned near the HOMO level in the energy gap. As a result, an ohmic contact for holes is formed at the interface (Fig. 1.3.5 (b)). However, if the W_m is lower than the LUMO level of the donor molecule, an energy barrier for holes is formed at the interface. In contrast, an ohmic contact for electrons at the acceptor layer/electrode interface requires that W_m < LUMO level of the acceptor molecule (Figs. 1.3.5 (c) (d)). The OSCs usually have a layer of high or low work function material inserted between an organic layer and an electrode make sufficient ohmic contact. On the other hand, a heavily doped layer also makes ohmic contact because the width of the depletion layer becomes less than 3 nm[45]. This narrow depletion layer allows charge to transport by tunneling.

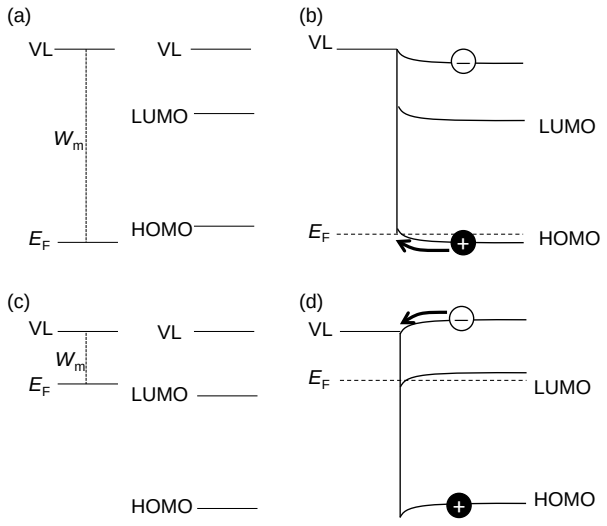

Fig. 1.3.5. Energy band diagram of a metal and an organic semiconductor. (a)(c) Before contact. (b)(d) After contact.

The alignment of the energy levels at the organic semiconductor/organic semiconductor interface is important because charge separation and recombination occurs at the donor/acceptor interface. Electron transfer from donor to acceptor occurs at the donor/acceptor interface[46]. As a result, the vacuum level in the acceptor layer is higher than that in the donor layer (Fig. 1.3.6. (b)). Alignment of these energy levels suggests that there is an interfacial dipole at the interface. However, neither cation nor anion species have been observed at the interface[47]. Recently, an electrostatic model has been applied to organic semiconductor/organic semiconductor interfaces[47–49]. This model assumes that there is an electrostatic field from the substrate to the interface, i.e. not only an interfacial dipole at the donor/acceptor interface. The change in the gradient of the vacuum level is due to the electrostatic field between the substrate and the door/acceptor interface (Fig. 1.3.6. (d))

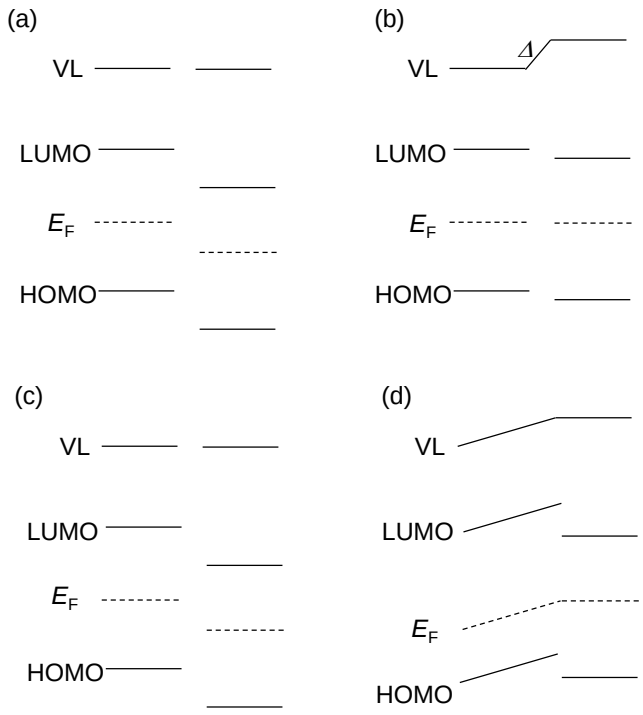

Fig. 1.3.6. Energy band diagram of the donor and acceptor molecules. (a)(c)Before contact. (b) Interfacial dipole model (d) Electrostatic model.

1.4. Device performance of organic solar cells

The power conversion efficiency (PCE) is determined by the *J*-*V* curve. This curve is measured under air mass 1.5, with a light intensity of 100 mW cm^{-2}. This condition corresponds to irradiation of the surface of the earth by sunlight at an incident angle of 48.2°. A typical *J*-*V* curve is shown in Fig 1.3.7. The PCE is determined by the following equation:

$$\mathrm{PCE} = \frac{J_{MAX}V_{MAX}}{P_{\mathrm{int}}} = \mathrm{FF}\frac{J_{SC}V_{OC}}{P_{\mathrm{int}}}$$

Where P_{int} is the incident power density, J_{max} and V_{max} are the maximum values of the photo-current density and the voltage. FF is given by the following equation:

$$\mathrm{FF} = \frac{J_{MAX}V_{MAX}}{J_{SC}V_{OC}}$$

Thus, the device performance of the OSC is determined by three parameters: the short-circuit photo-current (J_{SC}), the open-circuit voltage (V_{OC}) and the fill factor (FF).

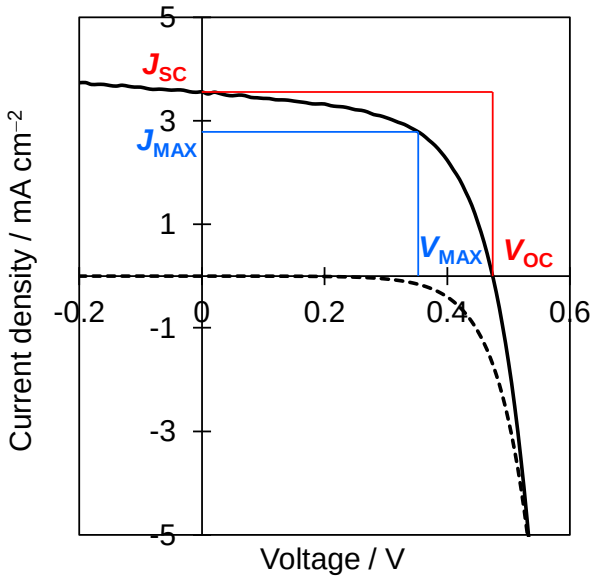

Fig. 1.3.7. Typical *J*-*V* curve of organic solar cell.

The *J-V* curve for a p-n junction cell under irradiation is given by the following equation:

$$J(V) = J_0\left(exp\left(\frac{eV}{nkT}\right) - 1\right) - J_{SC}$$

where J (V) is the photo-current density at the applied voltage V, J_0 is the saturation dark current density, e is the elementary charge, n is the ideality factor, and kT is the thermal energy. The series resistance and leakage current are neglected in this equation.

The open circuit voltage, V_{OC}, can be found by setting the photo-current density, $J(V)$, to zero in the above equation:

$$V_{OC} = n\frac{kT}{e}\ln\left(\frac{J_{SC}}{J_0} - 1\right)$$
$$\approx n\frac{kT}{e}\ln\left(\frac{J_{SC}}{J_0}\right)$$

According to this equation, V_{OC} increases with increasing J_{SC}. J_{SC} is related to the total charge collected per incident photon. In contrast, V_{OC} decreases with increasing J_0. J_0 is represented by the recombination current in the dark. Thus, charge recombination causes J_{SC}, V_{OC} and FF to decrease.

1.5. Current issues in organic solar cells

The performance of organic solar cells is related to the charge carrier transport and recombination. Charge generation in the co-deposited film is sufficient because the excitons reach the donor/acceptor interface immediately. The ideal morphology for the co-deposited film is that the donor and acceptor regions are arranged alternately. This morphology ensures the charge carrier transport pathway. However, fabrication of an ideal co-deposited film is difficult. Thus, understanding the charge carrier transport properties in co-deposited films is important.

The open-circuit voltage (V_{OC}) is dependent on the energy difference (E_{DA}) between the HOMO level of the donor and LUMO level of the acceptor. However, the observed V_{OC} is significantly lower than E_{DA}. As mentioned earlier, the lower V_{OC} is related to charge recombination. In order to increase V_{OC}, we need to understand the relationship between V_{OC} and charge recombination.

1.6. Motivation for this thesis

In this thesis, the author has focused on clarifying the effects of the charge carrier behavior on the performance of an OSC.

Firstly, the author attempted to clarify the charge transport properties in a co-deposited film. A mixed structure with both donor and acceptor molecules prevents charge carrier transport. If the range of the charge carriers is less than the thickness of the co-deposited film, the charge collection will be insufficient for the OSC. The author has estimated the range of the charge carriers in co-deposited films using impedance spectroscopy.

Next, the author focused on the relationship between carrier recombination and the reduction in V_{OC}. Since disorder causes trap-assisted recombination, the effect of trap-assisted recombination on V_{OC} should be clarified. The author attempted to show the presence of trap-assisted recombination in the OSCs. Moreover, the reduction in V_{OC} caused by trap-assisted recombination was quantified.

Finally, the author attempted to increase V_{OC} using impurity doping. The author believes that the value of V_{OC} is sensitive to the energy band structure at the donor/acceptor interface. On the other hand, the work function of the organic semiconductor is controlled by the impurity doping. Thus, impurity doping may cause the energy level alignment at the donor/acceptor interface to change. Consequently, the author clarified the effect of impurity doping on the value of V_{OC}.

.

1.7. Overview of this thesis

This thesis consists of five chapters.

In chapter 1, the motivation for this study and the fundamental principles of OSCs are described. The charge carrier behavior in OSCs, including carrier transport and recombination are also described, as are the impurity doping and alignment of the energy levels.

In chapter 2, the hole and electron transport in phthalocyanine (H_2Pc):fullerene (C_{60}) co-deposited films is described. The author has focused on charge carrier transport in these co-deposited films. Hole- and electron-only devices were fabricated by inserting heavily doped layers acting as ohmic contacts for holes or electrons, respectively. The carrier mobility (μ), the deep trapping lifetime (τ), and the range (L) of the charge carriers, that is, the average distance that the injected carriers can move until they are captured by the deep traps, for holes and electrons were obtained selectively by impedance spectroscopy. The dependences of μ, τ and L on the H_2Pc:C_{60} ratio were also obtained. For hole-only devices, μ_h increases from 10^{-6} to 10^{-4} cm^2 V^{-1} s^{-1} and τ_h decreases from 10^{-4} to 10^{-6} s as the H_2Pc ratio is increased from 50% to 83%. For electron-only devices, μ_e increases from 10^{-4} to 10^{-2} cm^2 V^{-1} s^{-1} and τ_h decreases from 10^{-5} to 10^{-6} s as the C_{60} ratio is increased from 17% to 50%. Interestingly, L_h and L_e remain constant and independent of the H_2Pc:C_{60} ratio, with values of 0.34 and 9.4 μm, respectively, obtained.

Because of the amorphous nature of the H_2Pc:C_{60} co-deposited films, a multiple trapping model is used to explain these results. Since holes are captured and released by

shallow traps many times, μ_h is dominated by the number of shallow traps. The author proposes that the magnitude of the disorder in H_2Pc aggregates is related to the number of shallow traps. The number of shallow traps decreases with increasing H_2Pc ratio since the magnitude of disorder decreases as the H_2Pc ratio increases. Thus, μ_h increases with increasing amounts of H_2Pc. Higher μ_h shortens the time required for holes to reach the deep traps, i.e., the deep trapping lifetime (τ_h). The increase in μ_h and the decrease in τ_h cancel each other out, so L_h is independent of the H_2Pc ratio. This explanation is also valid for the observed dependences of μ_e, τ_e, and L_e on the C_{60} ratio.

L_h and L_e are far greater than the typical thickness of co-deposited layers in organic photovoltaic cells, which is around 100 nm. There is no recombination process between holes and electrons in the hole-only and electron-only devices. Thus, the author concluded that, under conditions without recombination, electrons and holes, photo-generated in H_2Pc:C_{60} co-deposited films, can be collected at the respective electrodes.

In chapter 3, the reasons for the loss in V_{OC} in H_2Pc/C_{60} devices are described. In the open-circuit condition, the photo-generated charge can be described by the equilibrium between charge transfer and charge separation at the interface between the donor and acceptor layers. The energy of the photo-generated charge under open-circuit conditions is given by the charge transfer energy (E_{CT}), which is equal to E_{DA} minus the exciton binding energy. If the recombination rate increases, the observed V_{OC} becomes lower than E_{CT}. To clarify the relationship between the loss in V_{OC} and the charge recombination process, the author determined the energy loss and the charge recombination properties.

The author fabricated planar heterojunction H_2Pc/C_{60} solar cells. Since E_{CT} is the

low temperature limit of V_{OC}, the temperature dependence of V_{OC} was examined. From this, E_{CT} was determined to be 1.34 eV. The loss in V_{OC} was also determined and found to be 0.87 eV (= $E_{CT} - qV_{OC}$). In an ideal solar cell, the loss in V_{OC} is due to bimolecular recombination only. However, the measured dependence of V_{OC} on the light intensity indicates that there is both bimolecular and trap-assisted recombination in the H_2Pc/C_{60} devices. From the results of the temperature and the light intensity dependences of V_{OC}, the energy lost due to bimolecular recombination was found to be 0.55 and that due to trap-assisted recombination was 0.32 eV.

The dependence of the recombination lifetime on the charge carrier concentration was estimated from a Cole-Cole impedance plot. The reaction order of the charge carrier recombination decreases as the temperature increases. A reaction order of 2 means only bimolecular recombination occurs, whereas larger numbers mean that trap-assisted recombination is also involved. The decrease in reaction order with temperature indicates that bimolecular recombination is likely to happen at higher temperatures because free charge is released from the traps.

The H_2Pc/C_{60} devices had a large loss in V_{OC} related to trap-assisted recombination. The temperature dependence of the reaction order revealed that charge trapped at localized states was the main cause of the fast recombination. If the number of localized states can be decreased, H_2Pc/C_{60} devices have the potential to have larger values of V_{OC}.

In chapter 4, controlling V_{OC} by impurity doping is described. The energy band structure near the interface between the donor and acceptor layers may change V_{OC} because alignment of the Fermi levels (E_F) after the different layers are brought into

contact leads to a vacuum level shift near the interface and a change in E_{DA}. The author envisaged that the energy band structure could be controlled by the impurity doping, as a result of which the E_F of the organic layer could be manipulated. The author applied impurity doping to the H_2Pc/C_{60} solar cells.

The doped H_2Pc/C_{60} devices showed that V_{OC} decreased to 0.36 V when MoO_3 was added to the H_2Pc layer as a *p*-type dopant, whereas it increased to 0.52 V with Cs_2CO_3 as an *n*-type dopant. Energy level mapping revealed that a vacuum level shift had occurred near the donor/acceptor interface in the direction of decreasing E_{DA} with *p*-type doping and increasing E_{DA} with *n*-type doping, corresponding to the changes in V_{OC}. To investigate the effect of impurity doping near the interface, the author fabricated a number of H_2Pc/doped H_2Pc/C_{60} tri-layer devices with different thicknesses for the thin doped H_2Pc layer. For doped H_2Pc layers from 5 to 10 nm, the V_{OC} changes gradually. The value of V_{OC} of devices with 10 nm thick doped H_2Pc is almost the same as those with 50 nm thick doped H_2Pc. The results indicate that V_{OC} is determined by the energy band structure within 10 nm of the interface between the donor and acceptor layers.

The results demonstrate that the value of V_{OC} in OSCs is determined by the energy band structure near the donor/acceptor interface. The results also showed that the energy band structure can be controlled through impurity doping and that V_{OC} can be increased by *n*-type doping. This impurity doping effect can be adapted to OSCs in general.

In chapter 5, a summary of this thesis and the conclusions drawn from it are presented. The future prospects are also given.

1.8.Reference

[1] A.K. Ghosh, D.L. Morel, T. Feng, R.F. Shaw, C.A. Rowe, Photovoltaic and rectification properties of Al/Mg phthalocyanine/Ag Schottky□barrier cells, J. Appl. Phys. 45 (1974) 230–236. doi:10.1063/1.1662965.

[2] A.K. Ghosh, T. Feng, Merocyanine organic solar cells, J. Appl. Phys. 49 (1978) 5982–5989. doi:http://dx.doi.org/10.1063/1.324566.

[3] D.L. Morel, A.K. Ghosh, T. Feng, E.L. Stogryn, P.E. Purwin, R.F. Shaw, et al., High□efficiency organic solar cells, Appl. Phys. Lett. 32 (1978) 495–497. doi:10.1063/1.90099.

[4] C.W. Tang, Two□layer organic photovoltaic cell, Appl. Phys. Lett. 48 (1986) 183–185. doi:10.1063/1.96937.

[5] J.E. Kroeze, T.J. Savenije, M.J.W. Vermeulen, J.M. Warman, Contactless Determination of the Photoconductivity Action Spectrum, Exciton Diffusion Length, and Charge Separation Efficiency in Polythiophene-Sensitized TiO 2 Bilayers, J. Phys. Chem. B. 107 (2003) 7696–7705. doi:10.1021/jp0217738.

[6] M. Hiramoto, H. Fujiwara, M. Yokoyama, Three□layered organic solar cell with a photoactive interlayer of codeposited pigments, Appl. Phys. Lett. 58 (1991) 1062–1064. doi:10.1063/1.104423.

[7] M. Hiramoto, H. Fujiwara, M. Yokoyama, P-I-N Like Behavior in Three-Layered Organic Solar Cells Having a Co-Deposited Interlayer of Pigments, J. Appl. Phys. 72 (1992) 3781–3787. doi:10.1063/1.352274.

[8] G. Yu, J. Gao, J.C. Hummelen, F. Wudl, A.J. Heeger, Polymer Photovoltaic Cells: Enhanced Efficiencies via a Network of Internal Donor-Acceptor Heterojunctions, Science (80-.). 270 (1995) 1789–1791.

doi:10.1126/science.270.5243.1789.

[9] C.Y. Yang, A.J. Heeger, Morphology of composites of semiconducting polymers mixed with C60, Synth. Met. 83 (1996) 85–88. doi:10.1016/S0379-6779(97)80058-6.

[10] W. Zhao, D. Qian, S. Zhang, S. Li, O. Inganäs, F. Gao, et al., Fullerene-Free Polymer Solar Cells with over 11% Efficiency and Excellent Thermal Stability, Adv. Mater. 28 (2016) 4734–4739. doi:10.1002/adma.201600281.

[11] H.J. Cho, Y.J. Kim, S. Chen, J. Lee, T.J. Shin, C.E. Park, et al., Over 10% efficiency in single-junction polymer solar cells developed from easily accessible random terpolymers, Nano Energy. 39 (2017) 229–237. doi:10.1016/j.nanoen.2017.06.051.

[12] C. Liu, C. Yi, K. Wang, Y. Yang, R.S. Bhatta, M. Tsige, et al., Single-junction polymer solar cells with over 10% efficiency by a novel two-dimensional donor-acceptor conjugated copolymer, ACS Appl. Mater. Interfaces. 7 (2015) 4928–4935. doi:10.1021/am509047g.

[13] J. Yun, W. Wang, T.S. Bae, Y.H. Park, Y.-C. Kang, D.-H. Kim, et al., Preparation of Flexible Organic Solar Cells with Highly Conductive and Transparent Metal-Oxide Multilayer Electrodes Based on Silver Oxide, ACS Appl. Mater. Interfaces. 5 (2013) 9933–9941. doi:10.1021/am401845n.

[14] S. Lee, Y. Lee, J. Park, D. Choi, Stitchable organic photovoltaic cells with textile electrodes, Nano Energy. 9 (2014) 88–93. doi:10.1016/j.nanoen.2014.06.017.

[15] M. Kaltenbrunner, M.S. White, E.D. Głowacki, T. Sekitani, T. Someya, N.S. Sariciftci, et al., Ultrathin and lightweight organic solar cells with high flexibility, Nat. Commun. 3 (2012) 770. doi:10.1038/ncomms1772.

[16] H. Jinno, K. Fukuda, X. Xu, S. Park, Y. Suzuki, M. Koizumi, et al., Stretchable and waterproof elastomer-coated organic photovoltaics for washable electronic textile applications, Nat. Energy. 2 (2017) 780–785. doi:10.1038/s41560-017-0001-3.

[17] V. Vohra, K. Kawashima, T. Kakara, T. Koganezawa, I. Osaka, K. Takimiya, et al., Efficient inverted polymer solar cells employing favourable molecular orientation, Nat. Photonics. 9 (2015) 403–408. doi:10.1038/nphoton.2015.84.

[18] Y. Zou, R.J. Holmes, Correlation between the Open-Circuit Voltage and Charge Transfer State Energy in Organic Photovoltaic Cells, ACS Appl. Mater. Interfaces. (2015) 150813150227005. doi:10.1021/acsami.5b03656.

[19] A. Wilke, J. Endres, U. Hörmann, J. Niederhausen, R. Schlesinger, J. Frisch, et al., Correlation between interface energetics and open circuit voltage in organic photovoltaic cells, Appl. Phys. Lett. 101 (2012). doi:10.1063/1.4769360.

[20] M. Knupfer, Exciton binding energies in organic semiconductors, Appl. Phys. A. 77 (2003) 623–626. doi:10.1007/s00339-003-2182-9.

[21] T.M. Clarke, J.R. Durrant, Charge Photogeneration in Organic Solar Cells, Chem. Rev. 110 (2010) 6736–6767. doi:10.1021/cr900271s.

[22] S.D. Baranovskii, H. Cordes, F. Hensel, Charge Carrier Transport in Disordered Organic Solids, Phys. Rev. B. 62 (2000) 7934. doi:10.1002/polb.10643.

[23] D. Monroe, Hopping in exponential band tails, Phys. Rev. Lett. 54 (1985) 146–149. http://prl.aps.org/abstract/PRL/v54/i2/p146_1 (accessed April 26, 2014).

[24] M.A. Lampert, R.B. Schilling, Current Injection in Solids: The Regional Approximation Method, Semicond. Semimetals. 6 (1970) 1–96. doi:10.1016/S0080-8784(08)62630-7.

[25] J. Fischer, W. Tress, H. Kleemann, J. Widmer, K. Leo, M. Riede, Exploiting diffusion currents at Ohmic contacts for trap characterization in organic semiconductors, Org. Electron. Physics, Mater. Appl. 15 (2014) 2428–2432. doi:10.1016/j.orgel.2014.06.029.

[26] F.W. Schmidlin, Theory of trap-controlled transient photoconduction, Phys. Rev. B. 16 (1977) 2362–2385. doi:10.1103/PhysRevB.16.2362.

[27] C. Deibel, V. Dyakonov, Polymer–fullerene bulk heterojunction solar cells, Rep. Prog. Phys. 73 (2010) 1–39. doi:10.1088/0034-4885/73/9/096401.

[28] J. D., G. Lucovsky, The Physics of Hydrogenated Amorphous Silicon II, Springer Berlin Heidelberg, Berlin, Heidelberg, 1984. doi:10.1007/3540128077.

[29] R.S. Crandall, Modeling of thin film solar cells: Uniform field approximation, J. Appl. Phys. 54 (1983) 7176–7186. doi:10.1063/1.331955.

[30] K. Takagi, S. Abe, T. Nagase, T. Kobayashi, H. Naito, Characterization of transport properties of organic semiconductors using impedance spectroscopy, J. Mater. Sci. Mater. Electron. 26 (2015) 4463–4474. doi:10.1007/s10854-015-3070-8.

[31] K. Takagi, T. Nagase, T. Kobayashi, H. Naito, Determination of deep trapping lifetime in organic semiconductors using impedance spectroscopy, Appl. Phys. Lett. 108 (2016) 53305. doi:10.1063/1.4941235.

[32] E. Barsoukov, J.R. Macdonald, Impedance Spectroscopy: Theory, Experiment, and Applications, John Wiley & Sons, Inc., Hoboken, NJ, USA, 2005. doi:10.1002/0471716243.

[33] G. Lakhwani, A. Rao, R.H. Friend, Bimolecular recombination in organic photovoltaics., Annu. Rev. Phys. Chem. 65 (2014) 557–81. doi:10.1146/annurev-

physchem-040513-103615.

[34] M. Kuik, L.J.A. Koster, G.A.H. Wetzelaer, P.W.M. Blom, Trap-Assisted Recombination in Disordered Organic Semiconductors, Phys. Rev. Lett. 107 (2011) 256805. doi:10.1103/PhysRevLett.107.256805.

[35] R. a. Street, M. Schoendorf, A. Roy, J.H. Lee, Interface state recombination in organic solar cells, Phys. Rev. B. 81 (2010) 205307. doi:10.1103/PhysRevB.81.205307.

[36] S.M. Sze, M.-K. Lee, Semiconductor Devices - Physics and Technology, 3rd edition, 3rd ed., John Wiley & Sons, New York, 2012.

[37] B. Lüssem, M. Riede, K. Leo, Doping of organic semiconductors, Phys. Status Solidi. 210 (2013) 9–43. doi:10.1002/pssa.201228310.

[38] M. Kröger, S. Hamwi, J. Meyer, T. Riedl, W. Kowalsky, A. Kahn, P-type doping of organic wide band gap materials by transition metal oxides: A case-study on Molybdenum trioxide, Org. Electron. 10 (2009) 932–938. doi:10.1016/j.orgel.2009.05.007.

[39] M.L. Tietze, P. Pahner, K. Schmidt, K. Leo, B. Lüssem, Doped organic semiconductors: Trap-filling, impurity saturation, and reserve regimes, Adv. Funct. Mater. 25 (2015) 2701–2707. doi:10.1002/adfm.201404549.

[40] Z. Shang, T. Heumueller, R. Prasanna, G.F. Burkhard, B.D. Naab, Z. Bao, et al., Trade-Off between Trap Filling, Trap Creation, and Charge Recombination Results in Performance Increase at Ultralow Doping Levels in Bulk Heterojunction Solar Cells, Adv. Energy Mater. (2016). doi:10.1002/aenm.201601149.

[41] C. Ohashi, Y. Shinmura, M. Kubo, M. Hiramoto, Effects of doping at the ppm

level in Simple n+p-homojunction organic photovoltaic cells, Org. Electron. 27 (2015) 151–154. doi:10.1016/j.orgel.2015.09.001.

[42] Y. Shen, A.R. Hosseini, M.H. Wong, G.G. Malliaras, How to make ohmic contacts to organic semiconductors, ChemPhysChem. 5 (2004) 16–25. doi:10.1002/cphc.200300942.

[43] J.C. BERNÈDE, ORGANIC PHOTOVOLTAIC CELLS: HISTORY, PRINCIPLE AND TECHNIQUES, J. Chil. Chem. Soc. 53 (2008) 1549–1564. doi:10.4067/S0717-97072008000300001.

[44] S. Braun, W.R. Salaneck, M. Fahlman, Energy-Level Alignment at Organic/Metal and Organic/Organic Interfaces, Adv. Mater. 21 (2009) 1450–1472. doi:10.1002/adma.200802893.

[45] M. Kubo, Y. Shinmura, N. Ishiyama, T. Kaji, M. Hiramoto, Invertible organic photovoltaic cells with heavily doped organic/metal ohmic contacts, Appl. Phys. Express. 5 (2012) 92302. doi:10.1143/APEX.5.092302.

[46] Z.-L. Guan, J.B. Kim, H. Wang, C. Jaye, D.A. Fischer, Y.-L. Loo, et al., Direct determination of the electronic structure of the poly(3-hexylthiophene):phenyl-[6,6]-C61 butyric acid methyl ester blend, Org. Electron. 11 (2010) 1779–1785. doi:10.1016/j.orgel.2010.07.023.

[47] K. Akaike, N. Koch, M. Oehzelt, Fermi level pinning induced electrostatic fields and band bending at organic heterojunctions, Appl. Phys. Lett. 105 (2014) 223303. doi:10.1063/1.4903360.

[48] M. Oehzelt, K. Akaike, N. Koch, G. Heimel, Energy-level alignment at organic heterointerfaces, Sci. Adv. 1 (2015) e1501127–e1501127. doi:10.1126/sciadv.1501127.

[49] A. Opitz, Energy level alignment at planar organic heterojunctions: influence of contact doping and molecular orientation, J. Phys. Condens. Matter. 29 (2017) 133001. doi:10.1088/1361-648X/aa5a6c.

Chapter 2:

Hole- and electron-only transport in ratio-controlled organic co-deposited films observed by impedance spectroscopy

"Hole- and electron-only transport in ratio-controlled organic co-deposited films observed by impedance spectroscopy" Naoto Shintaku, Seiichiro Izawa, Kenichiro Takagi, Hiroyoshi Naito, Masahiro Hiramoto, *Org. Electron.*, **50**, 515-520 (2017).

Abstract

The dependences of the mobility, the lifetime of deep traps and the range for hole- and electron-only devices on the ratio of metal-free phthalocyanine and fullerene in co-deposited films were measured by impedance spectroscopy. The ranges of the carriers were shown to be independent of the ratio of the co-deposited molecules. A multiple trapping model in which the disorder of the co-deposited molecules gives rise to shallow traps that dominate the mobility is proposed. Very long hole and electron ranges of 0.34 and 9.4 μm, which are long enough to extract carriers from co-deposited films in organic photovoltaic cells, were observed.

2.1. Introduction

Co-deposited films of small molecular organic semiconductors have been widely used as active layers in organic photovoltaic cells [1-9]. To efficiently collect photo-generated carriers at the electrodes, an understanding of the transport properties of the holes and electrons in these co-deposited films is essential.

Fortunately, impedance spectroscopy (IS) has been developed to estimate the carrier mobility [10,11] and the distribution of localized states [12,13]. Simultaneous measurement of the carrier mobility and the lifetime of deep traps, and determination of the carrier range (Schuweg) were recently developed by Takagi [14,15]. Although measurements of the distributions of localized states in co-deposited films in organic photovoltaic cells has been reported [16], determination of the mobility, the lifetime of deep traps, and the carrier range has not been done for both holes and electrons.

In this chapter, the author shows that impedance spectroscopy measurements of the carrier mobility, the deep trapping lifetime and the carrier range for both holes and electrons in ratio controlled metal-free phthalocyanine:fullerene (H_2Pc:C_{60}) co-deposited films which is the typical system for small molecular photovoltaic cells. Very long hole and electron ranges of 0.34 and 9.4 mm were observed.

2.2. Experimental

H_2Pc (Dainippon Ink & Chemicals) and C_{60} (Frontier Carbon, nano purple TL) were purified by single-crystal sublimation [7,17]. Fig. 2.3.1(a) and (b) show the structures of hole- and electron-only devices utilizing H_2Pc:C_{60} co-deposited films, respectively. In order to make ohmic contacts to collect the holes and electrons, the undoped H_2Pc:C_{60} films were sandwiched between heavily doped *p*-layers (p^+) (Fig. 2.3.1(a)) or heavily doped *n*-layers (n^+) (Fig. 2.3.1(b)). The H_2Pc:C_{60} films were formed by co-deposition on indium tin oxide (ITO) substrates at 10^{-5} Pa in a vacuum evaporator housed in a glove box (EpiTech Inc., ETVP-VG 100-SP/12ET12007) purged with N_2 gas (H_2O < 40 ppm, O_2 < 0.2 ppm) (Fig. 2.3.1(c)). The evaporation rate of H_2Pc was 0.1 nm s^{-1} and that of C_{60} was varied from 0.02 to 0.1 nm s^{-1}. The H_2Pc:C_{60} ratio (X%:Y%) is abbreviated as H_2Pc X% for the hole-only devices and as C_{60} Y% for the electron-only devices. The thicknesses of the hole- and electron-only devices were 200 and 1400 nm, respectively [18]. Heavily doped p^+ (50,000 ppm MoO_3 (Alfa Aeser)) and n^+ (10,000 ppm Cs_2CO_3 (Aldrich)) –layers (10 nm) were formed by three-component co-evaporation [19].

The IS measurements [10-16] were carried out using an impedance analyzer (Solartron analytical, Modulab XM) in the frequency range from 1 to 10^6 Hz. In order to obtain capacitancefrequency (*C-f*) curves, an a.c. voltage with amplitude of 100 mV on top of a DC voltage was applied to the devices. The organic films were not exposed to air at any time during both film deposition and the IS measurements (FIg. 2.3.1(d)).

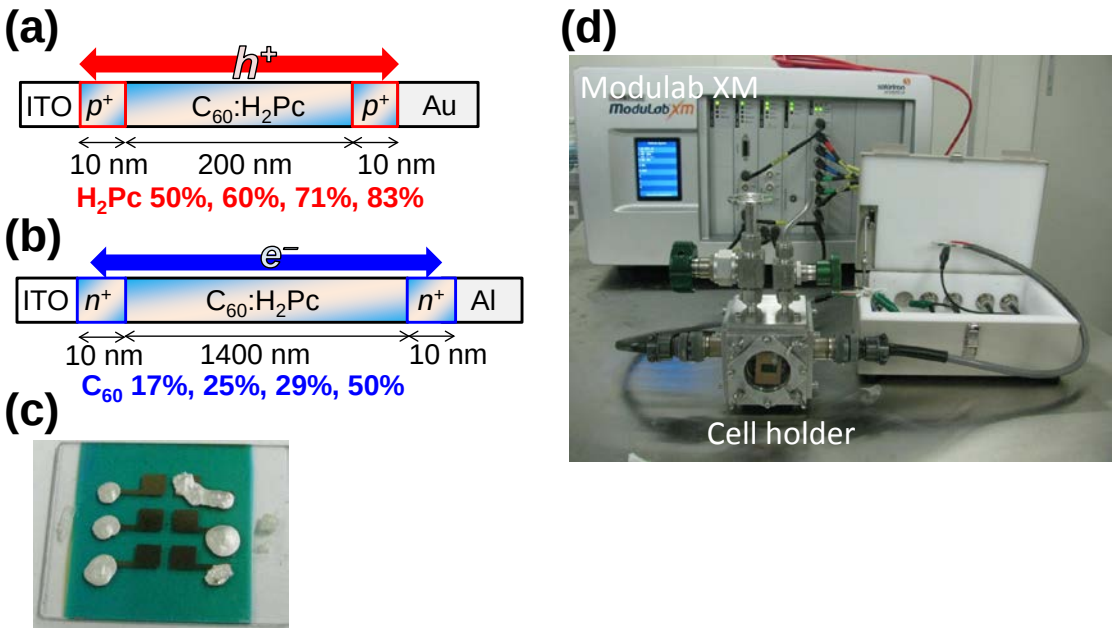

Fig. 2.3.1. (a) Hole-only device. (b) Electron-only device. (c) Fabricated device. (d) Impedance spectroscopy measurements, Modulab XM is connected to the device holder.

2.3. Results and discussion

2.3.1. *J-E* characteristics

Fig. 2.3.2 shows the current density-electric field (*J-E*) curves. All *J-E* curves were symmetric irrespective of the polarity of *E* [20]. For hole-only devices, by increasing the H_2Pc ratio from 50% to 83%, *J* increased around two orders of magnitude. For electron-only devices, by increasing C_{60} ratio from 17% to 29%, *J* increased three orders of magnitude. Observed *J-E* curves were completely different for hole- and electron-only devices.

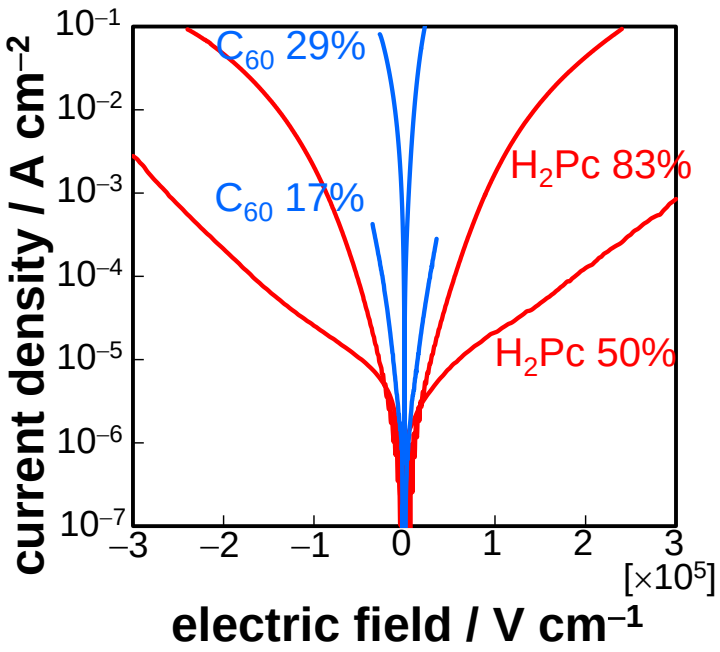

Fig. 2.3.2. *J-E* curves for hole-only devices (red curves) having H_2Pc 50% and 83% and for electron-only devices (blue curves) having C_{60}17% and 29%.

2.3.2. Hole-only devices

Fig. 2.3.3(a) shows the frequency dependence of the capacitance (*C-f* plot) for the hole-only H_2Pc 50% device (Fig. 2.3.1(a)). With V = 0 V, the capacitance (C) decreases monotonically (black curve). When a positive voltage (V) was applied to the ITO electrode, a clear valley-like response appeared in each *C-f* curve. On increasing the voltage from 1 to 8 V, the minimum value of C shifts from a low frequency (8.0×10^2 Hz at 1 V) to a high frequency (3.0×10^4 Hz at 8 V). Essentially the same results were obtained when applying the opposite polarity, i.e., a positive voltage to the Au electrode [20]. Inserting p^+-layers at the electrode interfaces (Fig. 2.3.1(a)), which makes both interfaces ohmic for holes, was necessary in order to obtain reproducible frequency response curves

The hole mobility (μ_h) can be obtained from the decrease in C on the high frequency side. Since C decreases due to discharge after the holes reach the counter electrode, the transit time (t_t) across the thickness (d) of the H_2Pc:C_{60} film is roughly equal to the reciprocal of the frequency at which C begins to decrease. μ_h can be obtained from the following equation.

$$\mu_h = \frac{d^2}{t_t V} \quad (1)$$

For a more precise determination of t_t, the frequency dependence of the negative differential susceptance ($-2\pi f\,(C-C_{geo})$), abbreviated here to $-\Delta B$, [10, 11, 21-25] was plotted (Fig. 2.3.3(e)). Here, C_{geo} is the geometrical capacitance. From the frequency (f_{max}) at which the maximum value of $-\Delta B$ occurs at V = 8 V, the transit time (t_t = 0.72 / f_{max}) and μ_h [11, 25, 26] were calculated to be 1.6×10^{-5} s and 4.3×10^{-6} $cm^2\ V^{-1}\ s^{-1}$ respectively. μ_h was shown to increase with electric field (E) (Fig. 2.3.4(a) black dots).

When the amount of H_2Pc was increased to 83% (Fig 2.3.3(f)), f_{max} shifted to higher frequencies. The carrier mobility is proportional to frequency; thus, μ_h increased from 10^{-6} cm^2 V^{-1} s^{-1} (H_2Pc 50%) to 10^{-4} cm^2 V^{-1} s^{-1} (H_2Pc 83%). On increasing the amount of H_2Pc, a systematic increase in μ_h was clearly observed (Fig. 2.3.5(a), dots).

The hole lifetime (τ_h) can be obtained from the increase in C on the low frequency side. C increases due to carriers being captured by deep traps before reaching the counter electrode [12, 25, 27]. We calculated τ_h using the numerical analysis developed by Takagi et al. [14]. For example, τ_h was determined to be 2.0×10^{-5} s for H_2Pc 50% at $V = 8$ V. τ_h was shown to decrease with E (Fig. 2.3.4(a) blue dots).

When the amount of H_2Pc was increased to 83% (Fig. 2.3.3(b)), the frequency at which C increased shifted to a higher value. τ_h is inversely proportional to frequency; thus, τ_h decreased from 1.4×10^{-4} s (H_2Pc 50%) to 4.3×10^{-6} s (H_2Pc 83%). On increasing the amount of H_2Pc, a systematic decrease in τ_h was clearly observed (Fig. 2.3.5(b), dots). Although there was finite distribution of lifetime data points due to the finite electric field range, there was far larger change in lifetime caused by varying H_2Pc ratio.

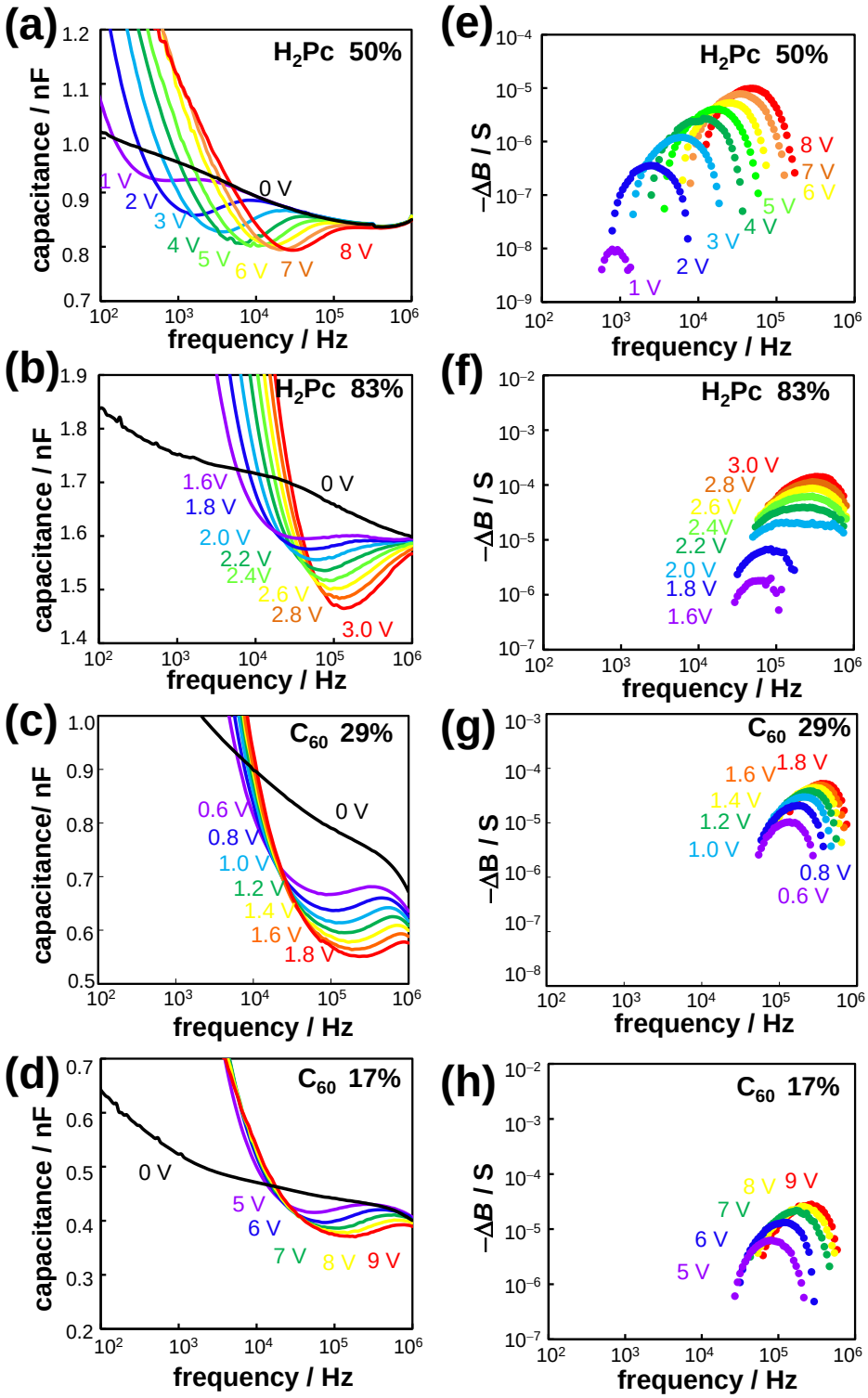

Fig. 2.3.3. Frequency dependences of the capacitance and $-\Delta B$ for hole-only devices of H_2Pc 50% (a) (e), H_2Pc 83% (b) (f) and for electron-only devices of C_{60} 50% (c) (g), C_{60}17% (d) (h). The applied d.c. voltage is shown in the figures.

2.3.3. Electron-only devices

Figs. 2.3.3(d) and 2.3.3(h) show the *C*-*f* and –Δ*B*-*f* plots for the electron-only C_{60} 17% (H_2Pc 83%) device (Fig. 2.3.1(b)). The observed μ_e for this device was determined to be 10^{-3} cm^2 V^{-1} s^{-1}, which is 10 times greater than the μ_h value (10^{-4} cm^2 V^{-1} s^{-1}) for the hole-only H_2Pc 83% device (Fig. 2.3.5(a)). The value of τ_e observed for the electron-only device was determined to be 10^{-5} s which is 10 times longer than the value of τ_h (10^{-6} s) for the hole-only device (Fig. 2.3.5(b)). Moreover, a systematic decrease in μ_e and a systematic increase in τ_e with decreasing C_{60} ratio were clearly observed (Figs. 2.3.5(a) and 2.3.5(b), triangles). Thus, the author successfully separately measured the mobility and lifetime for holes and electrons using IS.

2.3.4. Multiple trapping model

The author adopted the multiple trapping model (Fig. 2.3.4(b)) due to the amorphous nature of H_2Pc:C_{60} co-deposited films [28] and the mobility increase with E (Fig. 2.3.4(a) black dots) which indicate the existence of trap states. There are shallow and deep traps (red and black bars, respectively) for holes within the H_2Pc bandgap. Since the shallow traps are lying at low energy less than thermal energy at room temperature, holes are captured and released at shallow traps many times. Thus, μ_h is dominated by the shallow traps.

Finally, the holes are captured by deep traps, from which they are unable to escape. The time required for hole capture by the deep traps dominates the hole lifetime (deep trapping lifetime) (τ_h). The range (Schuweg) of the holes (L_h) is given by the following equation,

$$L_h = \mu_h \tau_h E \qquad (2)$$

The dependences of μ_h, τ_h and L_h on the electric field, E, for H_2Pc 50% are shown in Fig. 2.3.4(a). μ_h increased and τ_h decreased with increasing E and L_h was independent of E and had a constant value of 0.34 μm (Fig. 2.3.4(a)). These observed behavior can be reasonably explained by the multiple trapping model (Fig. 2.3.4(b)) [28]. The shallow traps dominate μ_h. The deep traps dominate L_h. Since the holes are more easily released from shallow traps at higher E, μ_h increase is observed (Fig. 2.3.4 (a) black dots). Since holes are hardly released from deep traps even at high E, constant L_h is observed. Thus, higher μ_h shortens the time required for holes to reach the deep traps, i.e., the deep trapping lifetime (τ_h).

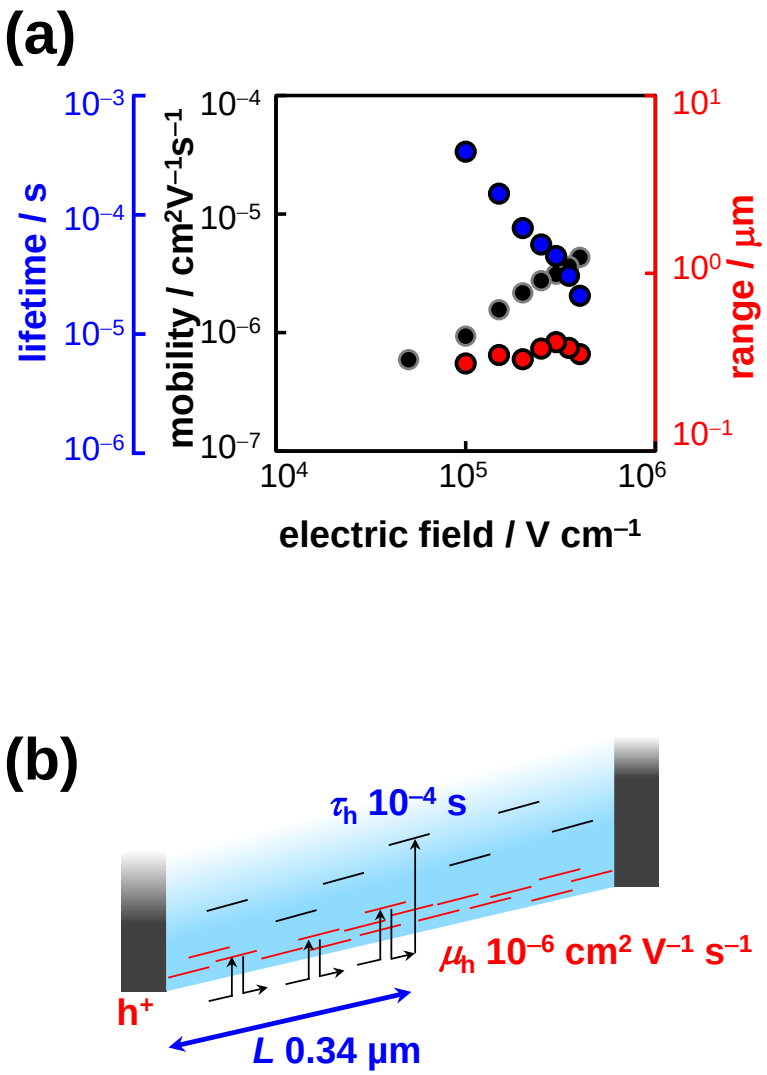

Fig. 2.3.4. (a) Electric field (E) dependences of the mobility (μ_h) (black dots), the deep trapping lifetime (τ_h) (blue dots), and the range (L_h) (red dots) for hole-only device of H_2Pc 50%. (b) Schematic illustrations of energetic structures near the upper edge of the H_2Pc valence band. The depth of the shallow hole traps is less than 0.025 eV at room temperature. The values of μ_h, τ_h and L_h at 1.0×10^5 V cm^{-1} are written in (b).

2.3.5. μ, τ, L dependences on the $H_2Pc:C_{60}$ ratio

For hole-only devices, μ_h increases from 10^{-6} to 10^{-4} cm^2 V^{-1} s^{-1} (Fig. 2.3.5(a) dots) and τ_h decreases from 10^{-4} to 10^{-6} s (Fig. 2.3.5(b), dots) as the H_2Pc ratio increases from 50% to 83%. Interestingly, L_h is independent of the H_2Pc concentration and has a constant value of 0.34 μm (Fig. 2.3.5(c), dots). For electron-only devices, μ_e increases from 10^{-4} to 10^{-2} cm^2 V^{-1} s^{-1} (Fig. 2.3.5(a), triangles) and τ_e decreases from 10^{-5} to 10^{-6} s (Fig. 2.3.5(b), triangles) as the amount of C_{60} increases from 17% to 50%. Again, L_e is independent of the concentration of C_{60} and has values around 9.4 μm (Fig. 2.3.5(c), triangles).

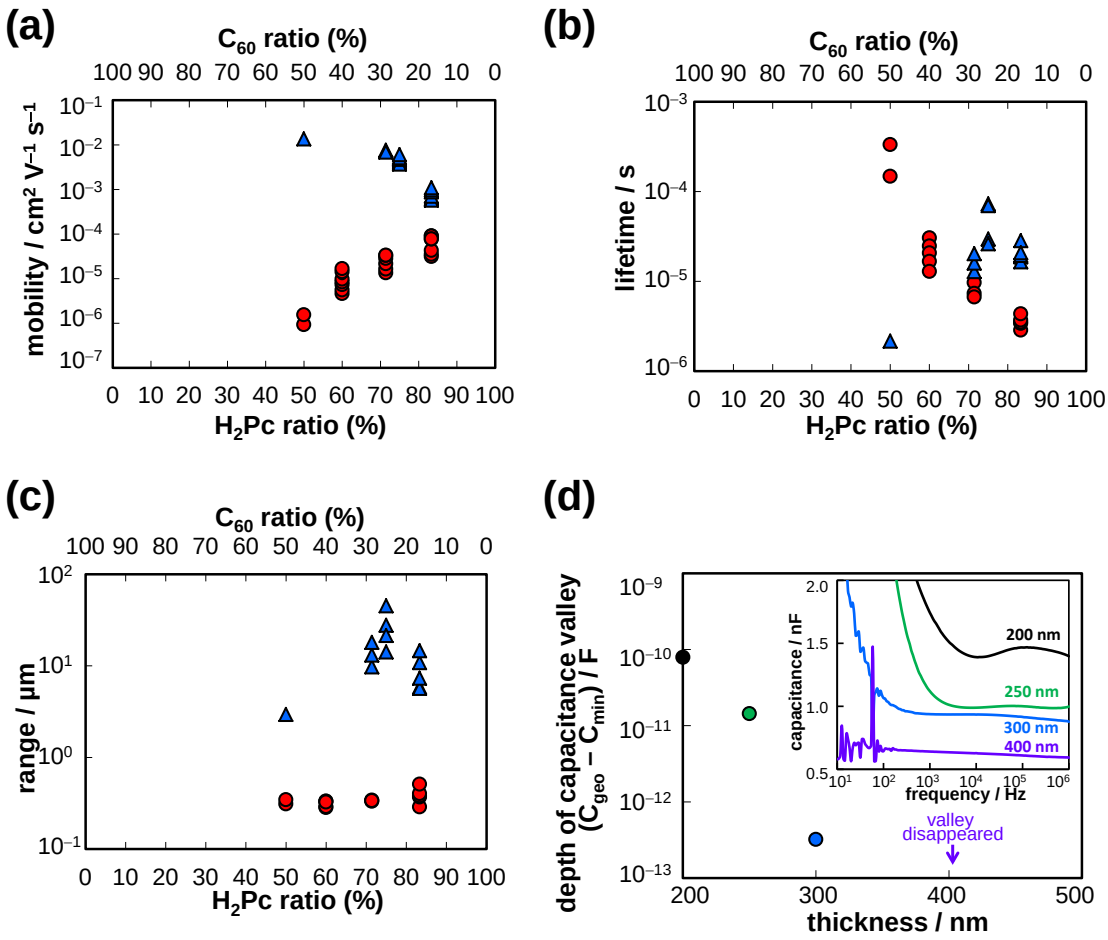

Fig. 2.3.5. Dependences of (a) mobility, (b) the deep trapping lifetime and (c) the range on the concentration of H_2Pc for hole-only devices (dots) and on the concentration of C_{60} for electron-only devices (triangles). Measurements for the hole-only and electron-only devices were made under electric fields in the ranges of 0.7 ~ 1.5 × 10^5 and 0.1 ~ 0.6 × 10^5 V cm^{-1}, respectively. (d) Dependence of the depth of valleys ($C_{geo} - C_{min}$ (C_{min}: minimum capacitance value of valley)) on the thickness (d) of H_2Pc 50% co-deposited films for hole-only devices at 1.5 × 10^5 V cm^{-1}. Inset: C-f curves for the hole-only devices having d of 200, 250, 300 and 400 nm.

2.3.6. Carrier transport in H_2Pc:C_{60} co-deposited film

Figs. 2.3.6(a) and 2.3.6(c) show a comparison between multiple trapping models for H_2Pc 50% and H_2Pc 83% hole-only devices. The increase in μ_h can be reasonably explained by the decrease in the number of shallow traps. Little X-ray diffraction peaks for H_2Pc or C_{60} were observed for H_2Pc 50%, this film can be regarded as being an amorphous mixture of H_2Pc and C_{60} molecules (Fig. 2.3.6(b)) [29]. We propose that the magnitude of the disorder in the H_2Pc aggregates can be considered to be related to the number of shallow traps. Since the magnitude of disorder of H_2Pc 83% is smaller than the 50% film, a higher value of μ_h was observed for the 83% film. On the other hand, L_h is independent of the H_2Pc:C_{60} ratio and has a constant value of 0.34 μm (Fig. 2.3.5(c), dots). This observation strongly suggests that L_h is dominated by the concentration of deep traps and is hardly influenced by the H_2Pc:C_{60} ratio. Thus, higher μ_h shortens the time required for holes to reach the deep traps, i.e., the deep trapping lifetime (τ_h). τ_h decrease with increasing H_2Pc composition is explained by the decrease of number of shallow traps. Actually, τ_h decreases from 10^{-4} to 10^{-5} s as the concentration of H_2Pc increases from 50% to 83%; that is, the increase in μ_h and the decrease in τ_h cancel each other out. We consider that the constant value of L_h, 0.34 μm, is inherent to amorphous H_2Pc. In the case of electron-only devices, μ_e increases and τ_e decreases as the concentration of C_{60} increases from 17% to 50% and the value of L_e of 9.4 μm remains roughly constant (Fig. 2.3.5(c), triangles). These results can be explained by the multiple trapping model for electrons in C_{60}, which is essentially the same as for holes in H_2Pc (Fig. 2.3.6). Since the average distance between the surface of C_{60} neighbors is 0.9 nm even in the diluted system (C_{60} 17%), C_{60} mediates the electron transport.

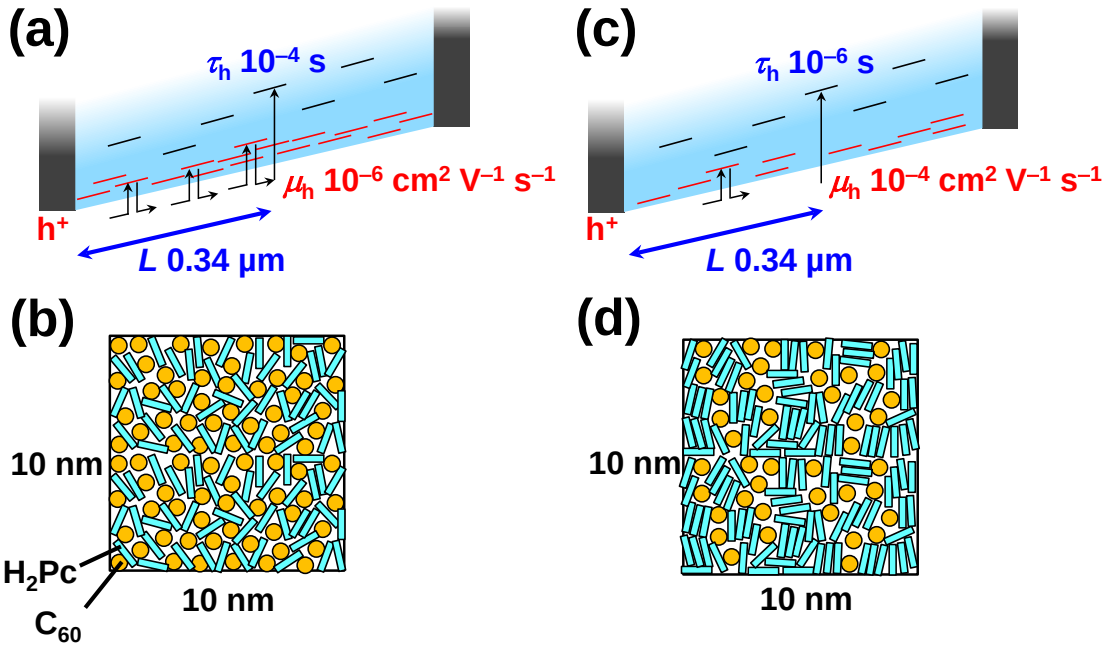

Fig. 2.3.6. Schematic illustrations of energetic structures near the upper edge of the H_2Pc valence band and microscopic structures (10 nm x 10 nm) for H_2Pc 50% (a) (b) and H_2Pc 83% (c) (d). The red and black bars correspond to shallow and deep trapping levels, respectively. The depth of the shallow hole traps is less than 0.025 eV at room temperature. The numbers of molecules were calculated taking account the density and the ratio of co-deposited films.

In order to clarify the effect of crystallization on L_h, a co-deposited H_2Pc:C_{60} film (H_2Pc 50%) was evaporated onto a substrate heated at 70 °C. This produces a film with many H_2Pc nanocrystals surrounded by amorphous C_{60} [30]. We obtained L_h = 1.6 μm which is longer than the value of 0.34 μm obtained for the amorphous H_2Pc film. Clearly, crystallization of the H_2Pc increases L_h. We surmise that the concentration of deep traps in crystalline H_2Pc is lower than that in amorphous H_2Pc.

The carrier range (L) can be determined experimentally by varying the distance between electrodes [31]. In order to clarify the physical meaning of L, we measured the thickness (d) dependence of *C-f* curves for hole-only devices (Fig. 2.3.5(d)). By increasing d from 200 to 400 nm (Fig. 2.3.5(d) inset), the depth of valleys in the *C-f* curves gradually decreased from 200 to 300 nm ($L>d$) and disappeared at 400 nm ($L<d$). Disappearance of capacitance valley clearly showed that the injected carriers could not reach to the opposite side electrode under the condition of $L<d$. The d value of the disappearance point of capacitance valley was in between 300 and 400 nm (Fig. 2.3.5(d)). Thus, L was directly determined by *C-f* curves. This was agreed with the value of range L = 0.34 μm which was calculated by using values of μ and τ. This experimental result showed that L has the clear physical meaning, i.e., the average distance that the injected carriers can move until they are captured by the deep traps [32].

2.4. Conclusions

In conclusion, the mobility, lifetime and range for holes and electrons were measured by IS using hole-only and electron-only devices. The observed hole and electron ranges (0.34 μm and 9.4 μm, respectively) under conditions without recombination were shown to be sufficiently long for carriers to be extracted from co-deposited films in organic photovoltaic cells with typical thicknesses of around 0.1 μm.

2.5. References

[1] S.S. Sun, N.S. Sariciftci (Eds.), Organic Photovoltaics, Mechanisms, Materials and Devices, CRC Press, New York, 2005.

[2] H. Spanggaard, F.C. Krebs, A brief history of the development of organic and polymeric photovoltaics, Sol. Energy Mater. Sol. Cells 83 (2004) 125. doi: 10.1016/j.solmat.2004.02.021.

[3] H. Hoppe, N.S. Sariciftci, Prospective Comparison of Contrast Enhanced CT Colonography and Conventional Colonoscopy for Detection of Colorectal Neoplasms in a Single Institutional Study Using Second-Look Colonoscopy with Discrepant Results, J. Mater. Res. 19 (2004) 1924. doi: 10.1111/j.1572-0241.2004.40238.x.

[4] F.C. Krebs (Ed.), Stability and Degradation of Organic and Polymer Solar Cells, John Wiley & Sons, Ltd., 2012.

[5] C.W. Tang, Two‐layer organic photovoltaic cell, Appl. Phys. Lett. 48 (1986) 183. doi: 10.1063/1.96937.

[6] M. Hiramoto, H. Fujiwara, M. Yokoyama, Three‐layered organic solar cell with a photoactive interlayer of codeposited pigments, Appl. Phys. Lett. 58 (1991) 1062. doi: 10.1063/1.104423.

[7] M. Hiramoto, M. Kubo, Y. Shinmura, N. Ishiyama, T. Kaji, K. Sakai, T. Ohno, M. Izaki, Bandgap Science for Organic Solar Cells, Electronics 3 (2014) 351. doi: 10.3390/electronics3020351.

[8] T. Kaji, M. Zhang, S. Nakao, K. Iketaki, K. Yokoyama, C.W. Tang, M. Hiramoto, Co-evaporant Induced Crystalline Donor: Acceptor Blends in Organic Solar Cells, Adv. Mater. 23 (2011) 3320. doi: 10.1002/adma.201101305.

[9] C. Ohashi, Y. Shinmura, M. Kubo, M. Hiramoto, Effects of doping at the ppm level in Simple n^+p-homojunction organic photovoltaic cells, Org. Electron. 27 (2015) 151. doi: 10.1016/j.orgel.2015.09.001.

[10] S.W. Tsang, S.K. So, J.B. Xu, Application of admittance spectroscopy to evaluate carrier mobility in organic charge transport materials, J. Appl. Phys. 99 (2006) 13706. doi: 10.1063/1.2158494.

[11] T. Okachi, T. Nagase, T. Kobayashi, H. Naito, Determination of Charge-Carrier Mobility in Organic Light-Emitting Diodes by Impedance Spectroscopy in Presence of Localized States, Jpn. J. Appl. Phys. 47 (2008) 8965. doi: 10.1143/JJAP.47.8965.

[12] T. Okachi, T. Nagase, T. Kobayashi, H. Naito, Determination of localized-state distributions in organic light-emitting diodes by impedance spectroscopy, Appl. Phys. Lett. 94 (2009) 43301. doi: 10.1063/1.3073043.

[13] J.A. Carr, M. Elshobaki, S. Chaudhary, Deep defects and the attempt to escape frequency in organic photovoltaic materials, Appl. Phys. Lett. 107 (2015) 203302. doi: 10.1063/1.4936160.

[14] K. Takagi, T. Nagase, T. Kobayashi, H. Naito, Determination of deep trapping lifetime in organic semiconductors using impedance spectroscopy, Appl. Phys. Lett. 108 (2016) 53305. doi: 10.1063/1.4941235.

[15] K. Takagi, S. Abe, T. Nagase, T. Kobayashi, H. Naito, Characterization of transport properties of organic semiconductors using impedance spectroscopy, J. Mater. Sci. Mater. Electron. 26 (2015) 4463. doi: 10.1007/s10854-015-3070-8.

[16] J. Fischer, D. Ray, H. Kleemann, P. Pahner, M. Schwarze, C. Koerner K. Vandewal, K. Leo, Density of states determination in organic donor-acceptor

blend layers enabled by molecular doping, J. Appl. Phys. 117 (2015) 245501. doi: 10.1063/1.4922587.

[17] R. Laudise, C. Kloc, P. Simpkins, T. Siegrist, Physical vapor growth of organic semiconductors, J. Cryst. Growth. 187 (1998) 449. doi: 10.1016/S0022-0248(98)00034-7.

[18] The thickness of C_{60} 50% film was 1000 nm.

[19] Bottom-side heavily doped and non-doped co-deposited layer covered the whole surface of ITO substrate. The area of upper-side heavily doped layer and metal electrode (100 nm) were the same (2 mm × 2 mm).

[20] Although the devices have the lager area of heavily doped layer at bottom-side than those at upper-side under metal electrode, the effects of in-plain conductivity due to the bottom-side heavily doped layer are negligible.

[21] H.C.F. Martens, J.N. Huiberts, P.W.M. Blom, Simultaneous measurement of electron and hole mobilities in polymer light-emitting diodes, Appl. Phys. Lett. 77 (2000) 1852. doi: 10.1063/1.1311599.

[22] H.C.F. Martens, W.F. Pasveer, H.B. Brom, J.N. Huiberts, P.W.M. Blom, Crossover from space-charge-limited to recombination-limited transport in polymer light-emitting diodes, Phys. Rev. B. 63 (2001) 125328. doi: 10.1103/PhysRevB.63.125328.

[23] K.L. Tong, S.W. Tsang, K.K. Tsung, S.C. Tse, S.K. So, Hole transport in molecularly doped naphthyl diamine, J. Appl. Phys. 102 (2007) 093705. doi: 10.1063/1.2804109.

[24] K.K. Tsung, S.K. So, Advantages of admittance spectroscopy over time-of-flight technique for studying dispersive charge transport in an organic semiconductor,

J. Appl. Phys. 106 (2009) 83710. doi: 10.1063/1.3251409.

[25] J.M. Montero, J. Bisquert, Interpretation of trap-limited mobility in space-charge limited current in organic layers with exponential density of traps, J. Appl. Phys. 110 (2011) 43705. doi: 10.1063/1.3622615.

[26] For $-\Delta B$-f analysis, modified equation $\mu = (4/3)\ (d^2 / t_t\ V)$ was used.

[27] S. Ishihara, H. Hase, T. Okachi, H. Naito, Bipolar carrier transport in tris(8-hydroxy-quinolinato) aluminum observed by impedance spectroscopy measurements, Org. Electron. 12 (2011) 1364. doi: 10.1016/j.orgel.2011.05.004.

[28] H. Naito, Y. Kanemitsu, Relations between transient charge transport and the glass-transition temperature in amorphous chalcogenides, Phys. Rev. B, 49 (1994) 49. doi: 10.1103/PhysRevB.49.10131.

[29] Although an extremely weak peak for crystalline H_2Pc, corresponding to a size of about 15 nm, was observed for H_2Pc 83%, the peak intensity was two orders of magnitude lower than that of a single film of H_2Pc.

[30] K. Suemori, T. Miyata, M. Yokoyama, M. Hiramoto, Three-layered organic solar cells incorporating a nanostructure-optimized phthalocyanine:fullerene codeposited interlayer, Appl. Phys. Lett. 86 (2005) 63509. doi: 10.1063/1.1863451.

[31] M. Kikuchi, K. Takagi, H. Naito, M. Hiramoto, Single crystal organic photovoltaic cells using lateral electron transport, Org. Electron. 41 (2017) 118. doi: 10.1016/j.orgel.2016.12.001.

[32] M.A. Lampert, P. Mark, Current Injection in Solids, Academic, New York, 1970, 150–152.

Chapter 3:

Effect of trap-assisted recombination on open-circuit voltage loss in phthalocyanine/fullerene solar cells

"Effect of trap-assisted recombination on open-circuit voltage loss in phthalocyanine/fullerene solar cells" Naoto Shintaku, Masahiro Hiramoto, Seiichiro Izawa, *Org. Electron*., in press. DOI:10.1016/j.orgel.2018.01.016.

Abstract

Large energy losses in open-circuit voltage (V_{OC}) are still an issue for the photo-conversion efficiency of organic solar cells (OSCs). The author clarifies the relationship between charge recombination and V_{OC} loss for phthalocyanine/fullerene planar heterojunction (PHJ) OSCs. The author quantifies the V_{OC} loss relative to the charge-transfer state energy by the temperature dependence of V_{OC}. The charge recombination order obtained from impedance measurements indicates the presence of trap-assisted recombination. Our results suggest that the V_{OC} losses are caused by the broad distribution of the tail state near the donor/acceptor (D/A) interface in the PHJ device. Thus, reducing the number of trap states near the D/A interface could lead to an increase in V_{OC}.

3.1. Introduction

Open-circuit voltage (V_{OC}) is an important parameter in determining the performance of organic solar cells (OSCs) [1]. It depends primarily on the energy level difference (E_{DA}) between the highest occupied molecular orbital (HOMO) of the electron donor material (D) and the lowest unoccupied molecular orbital (LUMO) of the electron acceptor material (A) [2]. However, the observed value of eV_{OC} (where e is the elementary charge) is always much lower than E_{DA}[3], and the consequent energy loss has been identified as a significant issue that hinders OSC performance.

In the open-circuit condition, the photo-generated charges are described as an equilibrium between the charge transfer and charge separated states at the donor/acceptor (D/A) interface[4]. The charge-transfer state energy (E_{CT}) is equal to E_{DA} minus the coulomb binding energy[4,5]. However, the photo-generated charges decay to the ground state through charge recombination, which causes a loss of energy between E_{CT} and eV_{OC}; therefore, the charge recombination process is important for estimating the V_{OC} loss. In ideal solar cells, the V_{OC} loss is solely due to bimolecular recombination[6]. However, in OSCs, trap-assisted recombination also causes additional V_{OC} loss[7,8].

In this chapter, the author clarifies the relationships between the V_{OC} loss and the charge recombination process. The V_{OC} loss relative to the E_{CT} is quantified in a phthalocyanine (H_2Pc)/fullerene (C_{60}) planar-heterojunction (PHJ) cell that is a typical materials combination in OSCs. To investigate the origin of the V_{OC} loss in H_2Pc/C_{60} devices, the author estimates the ideality factor (n), which indicates the charge recombination type. In addition, the author observes the temperature dependence of the

charge recombination behavior by impedance spectroscopy. Finally, the author proposes a way to decrease the V_{OC} loss based on these experimental results.

3.2. Experimental

H_2Pc (Dainippon Ink & Chemicals) and C_{60} (Frontier Carbon, nano purple TL) were purified by single-crystal sublimation. The OSC devices were fabricated on indium tin oxide (ITO)-coated glass substrates (ITO thickness: 150 nm; sheet resistance: 10.3 Ω sq^{-1}; Techno Print). The MoO_3 hole-transporting layer (10 nm, 0.1 nm s^{-1}), H_2Pc donor layer (50 nm, 0.1 nm s^{-1}), C_{60} acceptor layer (50 nm, 0.1 nm s^{-1}), BCP electron-transport layer (15 nm, 0.1 nm s^{-1}), and Al electrodes (75 nm, 0.4 nm s^{-1}) were deposited by thermal evaporation under high vacuum (~10^{-5} Pa) in a vacuum evaporation system (VTS-350M, ULVAC) housed in a glove box (DSO-1.5S MS3-P, Miwa). The devices were characterized in a vacuum container for optical measurements (Epitech) without exposure to air.

The *J–V* characteristics of the devices were measured under simulated solar illumination (AM 1.5, 100 mW cm^{-2}) from a solar simulator based on a 300 W Xe lamp (HAL-320, Asahi Spectra) using a source meter (R6243, Advantest). The light intensity was calibrated with a standard silicon solar cell (CS-20, Asahi Spectra). The active area of the devices was defined using a 0.04 cm^2 photomask. The device temperature (40 °C to 0 °C) was controlled using a thermoelectric temperature controller (VICS). The picture of temperature and light intensity dependence measurements are shown in Fig. 3.3.1.

The impedance spectroscopy were carried out using an impedance analyzer (Solartron analytical, Modulab XM) in the frequency range from 1 to 10^6 Hz with amplitude voltage of 50 mV.

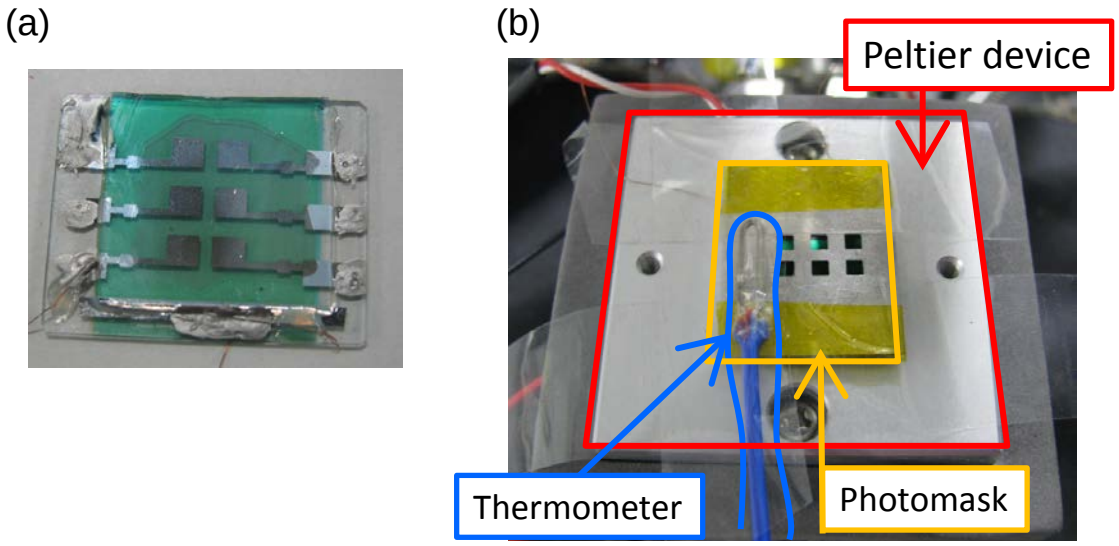

Fig. 3.3.1 (a) Sealed device. (b) Temperature and light intensity dependence measurement using Peltier device and thermometer.

3.3. Results and discussion

3.3.1. Temperature and light intensity dependence of V_{OC}

The PHJ device was fabricated by thermal evaporation under high vacuum, and had an ITO/MoO_3/H_2Pc/C_{60}/BCP/Al structure (Fig. 3.3.2(a)). The author measured a V_{OC} of 0.47 V, short-circuit current (J_{SC}) of 2.84 mA cm^{-2}, fill factor of 0.59, and power-conversion efficiency of 0.78% at room temperature under simulated solar illumination (AM 1.5, 100 mW cm^{-2}). These values are similar to those reported in previous studies[9,10].

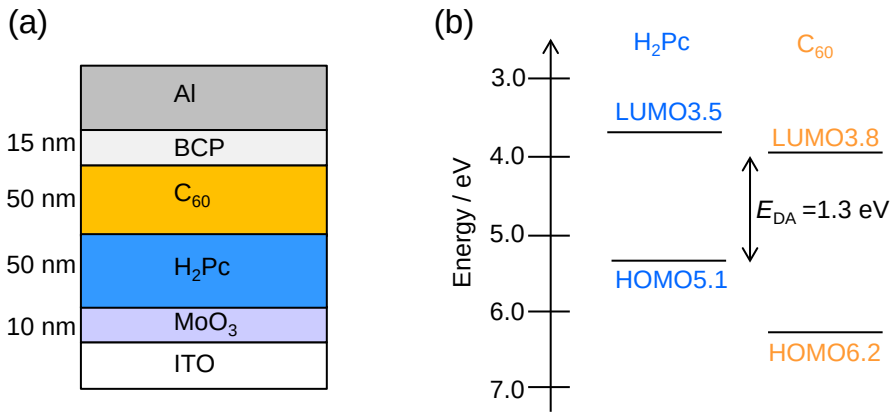

Fig. 3.3.2 Schematics of (a) the H_2Pc/C_{60} OSC device and the (b) H_2Pc and C_{60} energy levels.

The author estimated the V_{OC} loss relative to the E_{CT} values obtained from the temperature dependence of the J–V characteristics (Fig. 3.3.3(a)). Since the E_{CT} is a low temperature limit for the V_{OC}, the author can extract the E_{CT} values as the intercept of the linear plots of V_{OC} as a function of temperature[5]. The temperature dependence of V_{OC} was plotted in Fig. 3.3.3(b). This shows that V_{OC} decreased from 0.54 to 0.42 V as the temperature increased from 275 to 317 K. The change in V_{OC} with temperature can be expressed as follows:

$$eV_{OC} = E_{CT} - nkT\ln\left(\frac{J_{00}}{J_{ph}}\right)$$

where k is Boltzmann's constant, T is the temperature, J_{ph} is the photo-generated current density, and J_{00} is the pre-exponential factor of the reverse saturation current density. For the results shown in Fig. 3.3.3(b), this gives an E_{CT} of 1.34 eV, which is roughly equal to the E_{DA} for H_2Pc/C_{60}. As the energy loss between E_{CT} and eV_{OC} at room temperature was 0.87 eV, more than half of the energy was lost owing to charge recombination.

Next, to identify the type of charge recombination occurring in the OSC, the author estimated the ideality factor n from the light intensity dependence of the J–V characteristics shown in Fig. 3.3.3(c). Since the slope of the relationship between V_{OC} and the light intensity can be represented as nkT [11,12], the author can extract n from the slopes of these plots. In ideal p–n junctions where recombination is dominated by bimolecular recombination, i.e., band-to-band recombination, n is equal to unity. However, in classical p–n junctions, n has been reported to increase owing to Shockley–Read–Hall (SRH) recombination[13]. An n value greater than unity also indicates the presence of trap-assisted recombination in OSCs [14,15]. The relationship between light intensity and V_{OC} is plotted in Fig. 3.3.3(d), which shows that V_{OC} increased from 0.34 to 0.53 V as the light intensity increased from 5 to 400 mW cm^{-2}. The slope of a linear fit to this data gives n = 1.57, thus indicating the occurrence of both bimolecular and trap-assisted recombination in this PHJ device. Eq. 1 expresses the energy loss between E_{CT} and eV_{OC} in terms of n, k, T, J_{ph}, and J_{00}. The author calculated that $J_{00} = 7.19\times10^{9}$ mA cm^{-2} using the J_{SC} values for J_{ph}, obtained n values, and slope of the temperature dependence of V_{OC}. The value of J_{00} is related to the charge recombination rate [16]. The contributions of J_{00} and n to the V_{OC} loss are as follows [7]:

$$eV_{rec}\ \text{loss} = kT\ln\left(\frac{J_{\text{ph}}}{J_{00}}\right) \text{ and}$$

$$eV_{trap}\ \text{loss} = (n-1)kT\ln\left(\frac{J_{\text{ph}}}{J_{00}}\right).$$

The J_{ph}/J_{00} ratio corresponds to the balance between the charge generation and recombination rates. V_{rec} represents the energy loss in the ideal case where n is unity and V_{trap} represents the additional loss when n is greater than unity, i.e., the contribution of trap-assisted recombination. The values of V_{rec} and V_{trap} were calculated to be 0.55 and 0.32 V, respectively (Fig. 3.3.3(e)).

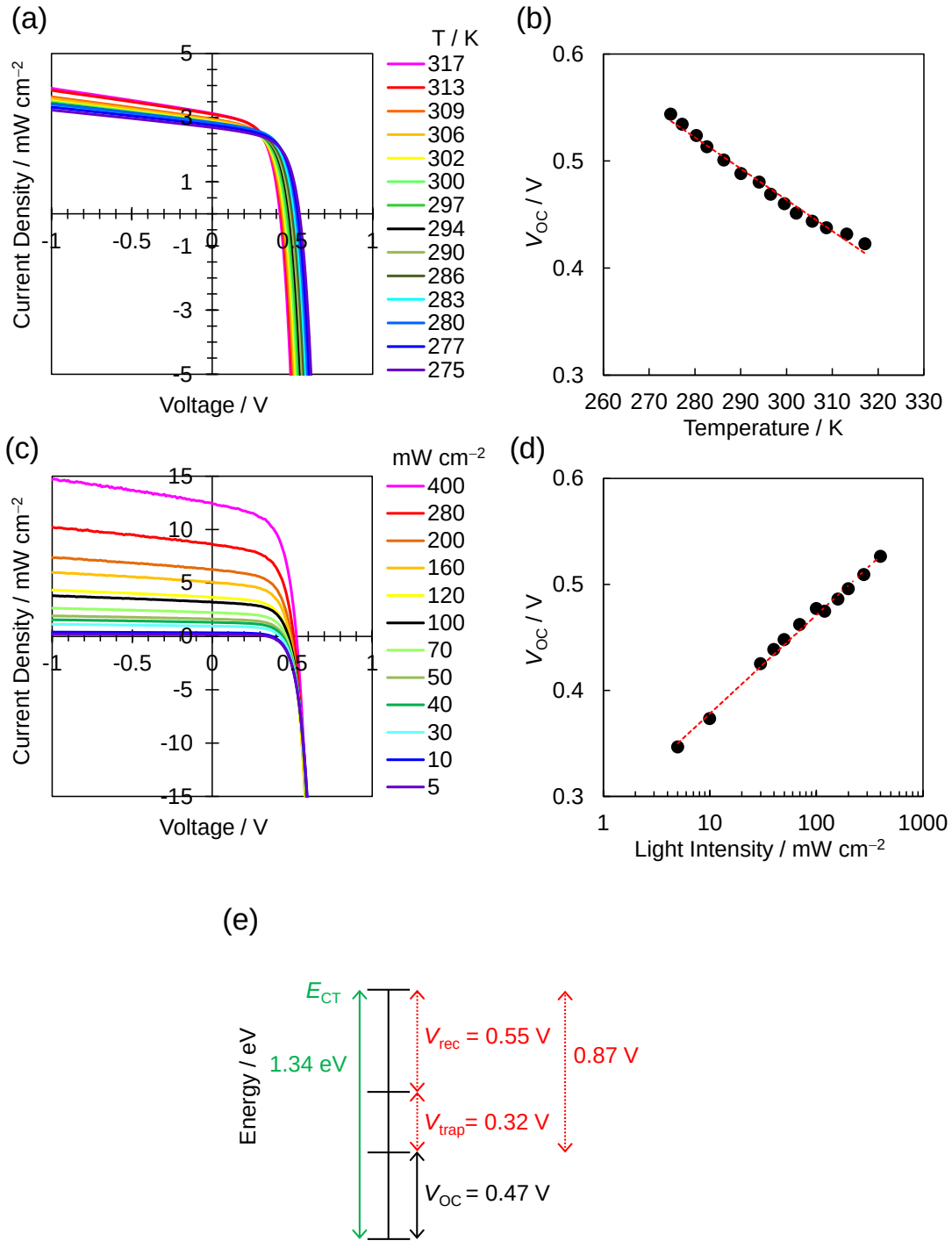

Fig. 3.3.3. (a) *J*–*V* curves for the H_2Pc/C_{60} OSC at various temperatures. (b) Temperature dependence of V_{OC}. (c) *J*–*V* curves for the H_2Pc/C_{60} OSC at various light intensities. (d) Light intensity dependence of V_{OC}. (e) Schematic diagram of the V_{OC} losses relative to E_{CT}.

3.3.2. Cole-Cole plot

To investigate the charge recombination process, the author performed impedance spectroscopy to obtain the recombination lifetime τ and carrier density N for the PHJ device. Cole-Cole plots were measured under various light intensities from 10 to 400 mW cm^{-2} with DC voltages equal to V_{OC} applying to the device, and the results are shown in Fig. 3.3.4(a). The observed capacitive semicircles are fitted using simple parallel RC elements as the active layer and a direct R as the contact resistance (Fig. 3.3.4(a), bottom) [17,18]. The fitting results are consistent with the experimental data. The recombination lifetime τ was calculated from the RC constant, and its light intensity dependence is shown in Fig. 3.3.4(b). The lifetime τ reduced from 27 to 1.4 μs as the intensity increased from 10 to 400 mW cm^{-2} because the probability of charge recombination increased with an increase in the light intensity. The carrier density that was calculated from the charge Q, which was given by the product of C and applied DC voltage, was divided by the active layer volume (Fig. 3.3.4(b)). The carrier density N increased with an increase in the light intensity owing to the increase in the number of photo-generated charge carriers.

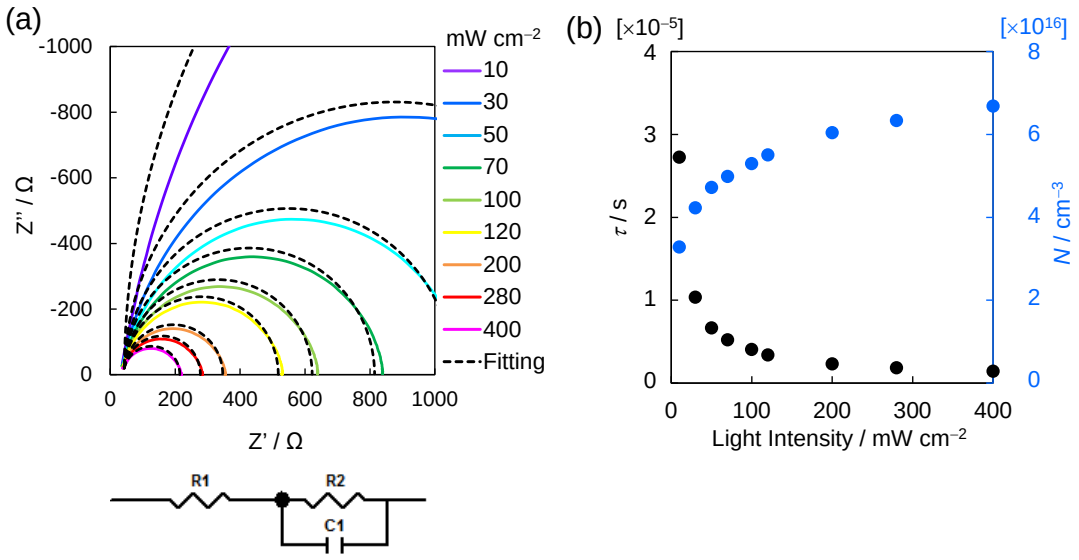

Fig. 3.3.4. (a) Cole–Cole plots for the H_2Pc/C_{60} OSC at various light intensities with DC voltages equal to V_{OC} applied to the device. The equivalent circuits used to fit the measured data are shown below the plots, and the fitting curves are plotted as broken lines. (b) Dependence of recombination lifetime and carrier density on light intensity determined by the Cole–Cole plot fitting results.

Next, the author confirms the validity of the τ and N values estimated by impedance spectroscopy by reproducing V_{OC}. By rearranging the diode equation, V_{OC} can be expressed in terms of the balance between the current generated by the light irradiation (J_{ph}) and the reverse saturation current, namely the recombination current in the dark (J_{rec0}), as follows:

$$eV_{OC} = nkT\ln\left(\frac{J_{ph}}{J_{rec0}}\right).$$

Thus, the value of V_{OC} can be reproduced by estimating J_{rec0}. The recombination current under light irradiation can be expressed as follows:

$$J_{rec} = edk_{rec}N^2,$$

where d is the thickness of the active layer and k_{rec} is the recombination rate constant. Previous studies have reported the following:

$$k_{rec} = \frac{1}{(1+\lambda)N\tau}$$

where λ is the reaction order [19–21]. The order λ was calculated from the power-law relationship between τ and N ($\tau = \tau_0 N^{-\lambda}$, where τ_0 is the pre-factor), as shown in Fig. 3.3.5(a). This leads to the following equation for J_{rec}:

$$J_{rec} = ed\frac{1}{(1+\lambda)}\frac{N}{\tau}.$$

Fig. 3.3.5(b) plots the estimated J_{rec} values as a function of V_{OC}, and J_{rec0} can be extracted from the value of J_{rec} at V_{OC} = 0 as it is the recombination current in the dark [19,22]. The author calculated V_{OC} values for a variety of light intensities using the estimated J_{rec0}, the measured n value, and J_{SC} for J_{ph}. These calculated values were consistent with the observations (Fig. 3.3.5(c)), thus demonstrating that the τ and N values estimated by impedance spectroscopy were reasonable.

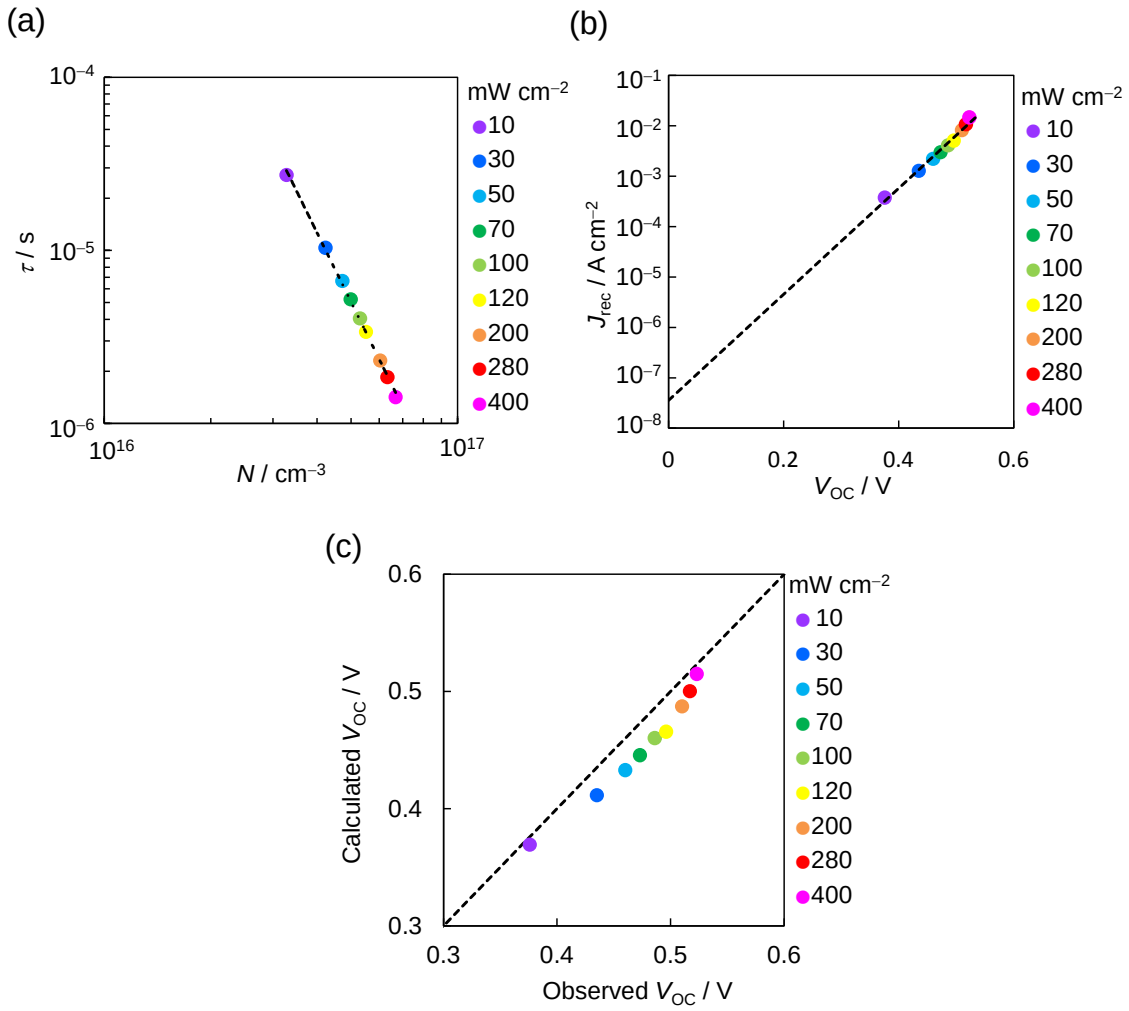

Fig. 3.3.5. (a) Recombination lifetime as a function of carrier density. (b) Recombination current density as a function of open-circuit voltage. (c) Calculated open-circuit voltage as a function of observed open-circuit voltage for various light intensities (10–400 mW cm^{-2}).

3.3.3. Temperature dependence of recombination order

To further investigate the process of charge recombination in the PHJ device, the author evaluated the temperature dependence of the recombination lifetime by impedance spectroscopy. Fig. 3.3.6(a) plots the recombination lifetime as a function of charge carrier density under various temperatures from 278 to 316 K. The power-law dependence of τ on N, i.e., the charge recombination reaction order, was 3.77 at room temperature (297 K). Previous studies have found that the recombination order of OSCs where only bimolecular recombination takes place is 2. However, when trap-assisted recombination is contained, the reaction order increases [14]. Such super-second-order kinetics can be explained by a reduction in the recombination rate caused by charges being trapped at tail states in an active layer. The λ over 2 is corresponding to the result of light intensity dependence of V_{OC} that shows the presence of trap-assisted recombination. The order decreased from 5.35 to 3.05 as the temperature increased (Fig. 3.3.6(b)), which can be explained by the behavior of the trapped charges. At low temperatures, trap-assisted recombination dominated the charge recombination process, but the trapped carriers were released from the trap states to become free charges at a high temperature. Thus, the charge recombination process was increasingly dominated by bimolecular recombination as the temperature increased, thus leading to the recombination order to approach 2. These results indicate that trapped charges play a key role in charge recombination and that the trap states are sufficiently shallow for the trapped charges to be released by thermal energy.

In the PHJ device used in the current study, charge recombination occurs only at the D/A interface; therefore, the trap states are due to the broad distributions of the tail state in either the H_2Pc or C_{60} layers near the D/A interface. The observed V_{OC}

values are sensitive to the energetic structure near the D/A interface; thus, reducing the number of nearby trap states is essential for increasing V_{OC}. The author believes that the traps can be filled by impurity doping or a highly crystalline D/A interface can lead to a decreased number of trap states, thus resulting in a low n value; this allows the V_{OC} loss to be reduced, i.e., V_{OC} to be increased.

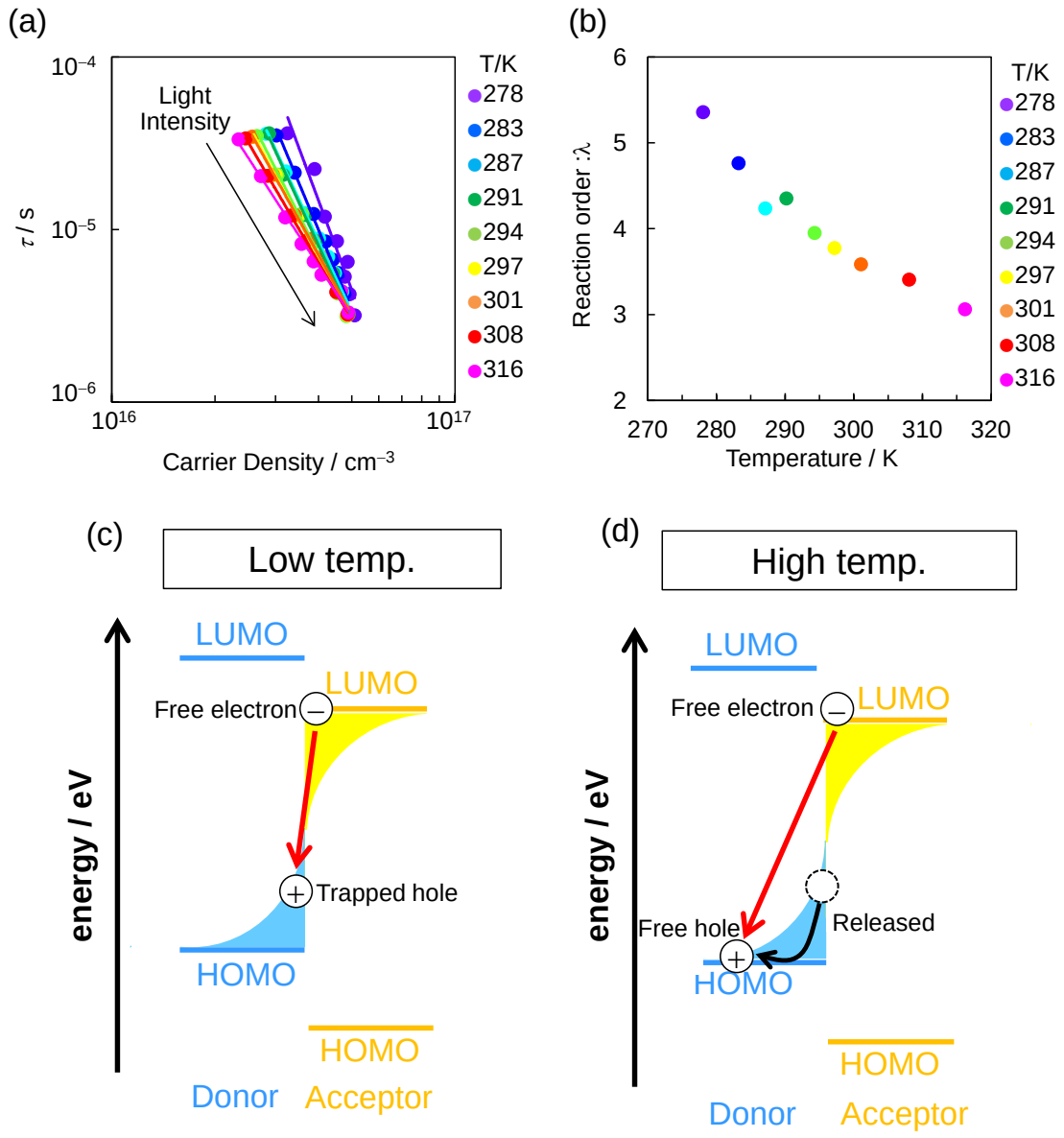

Fig. 3.3.6. (a) Recombination lifetime as a function of carrier density for various light intensities (5–100 mW cm^{-2}). (b) Recombination order as a function of temperature. (c), (d) Schematics of the charge recombination process at low and high temperatures, respectively. These show trapped holes recombining with free electrons, but trapped electrons can also recombine with free holes.

3.4. Conclusions

In this chapter, the author quantified the V_{OC} loss as 0.87 V and the ideal factor (n) as 1.57 by the temperature and light intensity dependence of the V_{OC} in an H_2Pc/C_{60} PHJ device. Since n was greater than unity, the presence of the trap-assisted recombination caused the additional V_{OC} loss. Furthermore, the charge recombination order decreased from 5.35 to 3.05 as the temperature increased, thus suggesting that the trapped charges were being released and becoming free charges. This indicates that trap states play a key role in charge recombination and the V_{OC} loss. Therefore, the author proposes that decreasing the number of trap states will lead to an increase in $V_{OC.}$

3.5. References

[1] H.-Y. Chen, J. Hou, S. Zhang, Y. Liang, G. Yang, Y. Yang, L. Yu, Y. Wu, G. Li, Polymer solar cells with enhanced open-circuit voltage and efficiency, Nat. Photonics. 3 (2009) 649–653. doi:10.1038/nphoton.2009.192.

[2] N.K. Elumalai, A. Uddin, Open circuit voltage of organic solar cells: an in-depth review, Energy Environ. Sci. 9 (2016) 391–410. doi:10.1039/C5EE02871J.

[3] U. Hörmann, J. Kraus, M. Gruber, C. Schuhmair, T. Linderl, S. Grob, S. Kapfinger, K. Klein, M. Stutzman, H.J. Krenner, W. Brütting, Quantification of energy losses in organic solar cells from temperature-dependent device characteristics, Phys. Rev. B - Condens. Matter Mater. Phys. 88 (2013) 1–13. doi:10.1103/PhysRevB.88.235307.

[4] T.M. Burke, S. Sweetnam, K. Vandewal, M.D. McGehee, Beyond Langevin recombination: How equilibrium between free carriers and charge transfer states determines the open-circuit voltage of organic solar Cells, Adv. Energy Mater. 5 (2015) 1–12. doi:10.1002/aenm.201500123.

[5] K. Vandewal, K. Tvingstedt, A. Gadisa, O. Inganäs, J. V. Manca, Relating the open-circuit voltage to interface molecular properties of donor:acceptor bulk heterojunction solar cells, Phys. Rev. B - Condens. Matter Mater. Phys. 81 (2010) 1–8. doi:10.1103/PhysRevB.81.125204.

[6] N.C. Giebink, G.P. Wiederrecht, M.R. Wasielewski, S.R. Forrest, Ideal diode equation for organic heterojunctions. I. Derivation and application, Phys. Rev. B. 82 (2010) 155305. doi:10.1103/PhysRevB.82.155305.

[7] S.D. Collins, C.M. Proctor, N.A. Ran, T.-Q. Nguyen, Understanding Open-Circuit Voltage Loss through the Density of States in Organic Bulk

Heterojunction Solar Cells, Adv. Energy Mater. 6 (2016) 1501721. doi:10.1002/aenm.201501721.

[8] M. Kuik, L.J.A. Koster, G.A.H. Wetzelaer, P.W.M. Blom, Trap-Assisted Recombination in Disordered Organic Semiconductors, Phys. Rev. Lett. 107 (2011) 256805. doi:10.1103/PhysRevLett.107.256805.

[9] M. Kubo, Y. Shinmura, N. Ishiyama, T. Kaji, M. Hiramoto, Invertible organic photovoltaic cells with heavily doped organic/metal ohmic contacts, Appl. Phys. Express. 5 (2012) 92302. doi:10.1143/APEX.5.092302.

[10] M. Hiramoto, M. Kubo, Y. Shinmura, N. Ishiyama, T. Kaji, K. Sakai, T. Ohno, M. Izaki, Bandgap Science for Organic Solar Cells, Electronics. 3 (2014) 351–380. doi:10.3390/electronics3020351.

[11] T. Kirchartz, F. Deledalle, P.S. Tuladhar, J.R. Durrant, J. Nelson, On the Differences between Dark and Light Ideality Factor in Polymer:Fullerene Solar Cells, J. Phys. Chem. Lett. 4 (2013) 2371–2376. doi:10.1021/jz4012146.

[12] L.J.A. Koster, V.D. Mihailetchi, R. Ramaker, P.W.M. Blom, Light intensity dependence of open-circuit voltage of polymer:fullerene solar cells, Appl. Phys. Lett. 86 (2005) 1–3. doi:10.1063/1.1889240.

[13] K.S. Nalwa, H.K. Kodali, B. Ganapathysubramanian, S. Chaudhary, Dependence of recombination mechanisms and strength on processing conditions in polymer solar cells, Appl. Phys. Lett. 99 (2011) 263301. doi:10.1063/1.3671999.

[14] J. Gorenflot, M.C. Heiber, A. Baumann, J. Lorrmann, M. Gunz, A. Kämpgen, V. Dyakonov, C. Deibel, Nongeminate recombination in neat P3HT and P3HT:PCBM blend films, J. Appl. Phys. 115 (2014) 144502. doi:10.1063/1.4870805.

[15] T. Kirchartz, B.E. Pieters, J. Kirkpatrick, U. Rau, J. Nelson, Recombination via tail states in polythiophene:fullerene solar cells, Phys. Rev. B. 83 (2011) 115209. doi:10.1103/PhysRevB.83.115209.

[16] S. Yamamoto, A. Orimo, H. Ohkita, H. Benten, S. Ito, Molecular Understanding of the Open-Circuit Voltage of Polymer:Fullerene Solar Cells, Adv. Energy Mater. 2 (2012) 229–237. doi:10.1002/aenm.201100549.

[17] A. Sánchez-Díaz, L. Burtone, M. Riede, E. Palomares, Measurements of Efficiency Losses in Blend and Bilayer-Type Zinc Phthalocyanine/C 60 High-Vacuum-Processed Organic Solar Cells, J. Phys. Chem. C. 116 (2012) 16384–16390. doi:10.1021/jp3054422.

[18] T.M. Clarke, C. Lungenschmied, J. Peet, N. Drolet, A.J. Mozer, A Comparison of Five Experimental Techniques to Measure Charge Carrier Lifetime in Polymer/Fullerene Solar Cells, Adv. Energy Mater. 5 (2015) 1401345. doi:10.1002/aenm.201401345.

[19] A. Maurano, R. Hamilton, C.G. Shuttle, A.M. Ballantyne, J. Nelson, B. O'Regan, W. Zhang, I. McCulloch, H. Azimi, M. Morana, C.J. Brabec, J.R. Durrant, Recombination dynamics as a key determinant of open circuit voltage in organic bulk heterojunction solar cells: A comparison of four different donor polymers, Adv. Mater. 22 (2010) 4987–4992. doi:10.1002/adma.201002360.

[20] A. Maurano, C.G. Shuttle, R. Hamilton, A.M. Ballantyne, J. Nelson, W. Zhang, M. Heeney, J.R. Durrant, Transient optoelectronic analysis of charge carrier losses in a selenophene/fullerene blend solar cell, J. Phys. Chem. C. 115 (2011) 5947–5957. doi:10.1021/jp109697w.

[21] C.G. Shuttle, B. O'Regan, A. M. Ballantyne, J. Nelson, D.D.C. Bradley, J. De

Mello, J.R. Durrant, Experimental determination of the rate law for charge carrier decay in a polythiophene: Fullerene solar cell, Appl. Phys. Lett. 92 (2008) 90–93. doi:10.1063/1.2891871.

[22] D. Credgington, J.R. Durrant, Insights from transient optoelectronic analyses on the open-circuit voltage of organic solar cells, J. Phys. Chem. Lett. 3 (2012) 1465–1478. doi:10.1021/jz300293q.

Chapter 4:

Controlling Open-Circuit Voltage in Organic Solar Cells by Impurity Doping

"Controlling open-circuit voltage in organic solar cells by impurity doping" Naoto Shintaku, Masahiro Hiramoto, Seiichiro Izawa, *J. Phys. Chem. C*, revising according to reviewers' comments.

Abstract

Impurity doping was applied to phthalocyanine (H_2Pc)/fullerene (C_{60}) planar heterojunction solar cells. The open-circuit voltage (V_{OC}) decreased to 0.36 V when a *p*-type dopant was added to the H_2Pc layer, whereas the V_{OC} increased to 0.52 V with an *n*-type dopant. Energy-level mapping revealed that the origin of the V_{OC} change was the vacuum level shifts occurring near the donor/acceptor (D/A) interface because of the Fermi-level alignment. The insertion of a thin doped H_2Pc layer at the D/A interface could avoid the deteriorative effect of *n*-type doping on charge transport in the bulk, resulting in an increase of the V_{OC} while maintaining short-circuit current density and fill factor. The results demonstrated that the V_{OC}s in organic solar cells are determined not only by the selection of D and A materials but also by the energy-level shift near the D/A interface that could be controlled by impurity doping.

4.1. Introduction

Open-circuit voltage (V_{OC}) is one of the most important parameters for determining the power conversion efficiency (PCE) of organic solar cells (OSCs).[1,2] The V_{OC} in OSCs is primary related to the energy-level difference between the highest occupied molecular orbital (HOMO) of an electron donor material and the lowest unoccupied molecular orbital (LUMO) of an electron acceptor material.[3] Previous reports have demonstrated that the eV_{OC} (e: elementary charge) is empirically expressed by the energy-level difference between the HOMO of the donor material and the LUMO of the acceptor material (E_{DA}), as measured by cyclic voltammetry minus 0.3 eV.[4] However, the E_{DA} in actual devices is sometimes changed because of the energy-level alignment at the donor/acceptor (D/A) interface. After different layers are contacted, charge transfer occurs between them to align the Fermi energy level (E_F) and the generated electrostatic field near the interface induces a vacuum-level (VL) shift.[5–7] The generated charges are also trapped at the gap state in the bulk, inducing band bending over a long range along the direction away from the interface.[8] The E_F alignment occurs at organic/organic interfaces as well as metal/organic interfaces. The V_{OC} in OSCs can be controlled if the energy-level shift near the D/A interface can be manipulated.

Impurity doping is one potential approach to controlling the energy-level shift near the D/A interface. The author have found that the E_F of an organic layer can be freely controlled by adding an appropriate dopant at an appropriate concentration.[9–11] The E_F of the films becomes deeper when a *p*-type dopant is added, whereas the E_F becomes shallower when an *n*-type dopant is added. Impurity doping has been intensively studied in the field of bulk heterojunction (BHJ)-type OSCs.[12–14] Shang

et al. have reported that the addition of a *p*-type dopant at a low concentration into solution-processed BHJ-OSCs filled the deep traps in the active layer and led to increases of approximately 0.3% and 0.02 V for the PCE and the V_{OC}, respectively.[14] However, the effect of impurity doping on the relationship between the energy-level alignment and the V_{OC} in OSCs has not been reported.

In the present study, impurity doping was applied to phthalocyanine (H_2Pc)/fullerene (C_{60}) planar heterojunction (PHJ) devices. The PHJ devices provide an advantage in investigating the effect of doping at the D/A interface because their flat and distinct interface enables us to observe energy-level shifts there.[15] Fig. 4.3.1(a) shows a schematic of the effects of impurity doping on the energy-level alignment. The E_F of the H_2Pc layer was controlled by both the dopant species and the concentration. After the doped H_2Pc and C_{60} layers are contacted, E_F alignment occurs, leading to a VL shift near the D/A interface. *p*-Type and *n*-type doping induce an energy-level shift in the directions of decreasing and increasing E_{DA}, respectively. The author hypothesized that the V_{OC} could be controlled by this effect.

4.2. Experimental

H_2Pc (Dainippon Ink & Chemicals) and C_{60} (Frontier Carbon, Nano Purple TL) were purified by single-crystal sublimation. MoO_3 (Alfa Aesar, 99.9995%) and Cs_2CO_3 (Sigma-Aldrich, 99.995%) were used as the acceptor and donor dopants, respectively. The OSC devices were fabricated on ITO-coated glass substrates (ITO thickness: 150 nm; sheet resistance: 10.3 Ω sq^{-1}; Techno Print). The MoO_3 hole-transporting layer (10 nm, 0.1 nm s^{-1}), H_2Pc donor layer (50 nm, 0.1 nm s^{-1}), C_{60} acceptor layer (50 nm, 0.1 nm s^{-1}), BCP electron-transport layer (15 nm, 0.1 nm s^{-1}), and Al electrodes (75 nm, 0.4 nm s^{-1}) were deposited via thermal evaporation under high vacuum (~10^{-5} Pa) in a vacuum evaporation system (VTS-350M, ULVAC) housed in a glove box (DSO-1.5S MS3-P, Miwa). The MoO_3 and Cs_2CO_3 as the dopant were introduced by co-deposition with H_2Pc or C_{60}. The devices were characterized in a vacuum container for optical measurements (Epitech) without exposure to air.

The *J*–*V* characteristics of the devices were measured under simulated solar illumination (AM 1.5, 100 mW cm^{-2}) from a solar simulator based on a 300-W Xe lamp (HAL-320, Asahi Spectra) using a source meter (R6243, Advantest). The light intensity was calibrated with a standard silicon solar cell (CS-20, Asahi Spectra). The active area of the devices was defined using a 0.04 cm^2 photomask. The position of the E_F was determined using a Kelvin probe (Riken-Keiki, FAC-1) in a glove box .

4.3. Results and discussion

4.3.1. Device performance of the doped H_2Pc/C_{60} device

The PHJ devices with a doped H_2Pc layer were fabricated by thermal evaporation under high vacuum. The structure of these devices was indium tin oxide (ITO)/MoO_3/doped H_2Pc/C_{60}/Bathocuproine (BCP)/Al (Fig. 4.3.1(b)). MoO_3 and Cs_2CO_3 were used as the *p*-type and *n*-type dopants, respectively.[9] The dopants were introduced into the H_2Pc layer via a co-deposition technique, and the dopant concentration relative to the H_2Pc volume was controlled by the ratio between the deposition rate of the dopant and that of the H_2Pc. The energy levels of the H_2Pc, C_{60}, MoO_3, and Cs_2CO_3 are summarized in Fig. 4.3.1(c). The work function (W_F) of the 50 nm H_2Pc films on ITO was 4.20 eV in the nondoped film, became deeper (4.56 eV) in the film doped with 2,000 ppm MoO_3, and became shallower (3.52 eV) in the film doped with 2,000 ppm Cs_2CO_3.

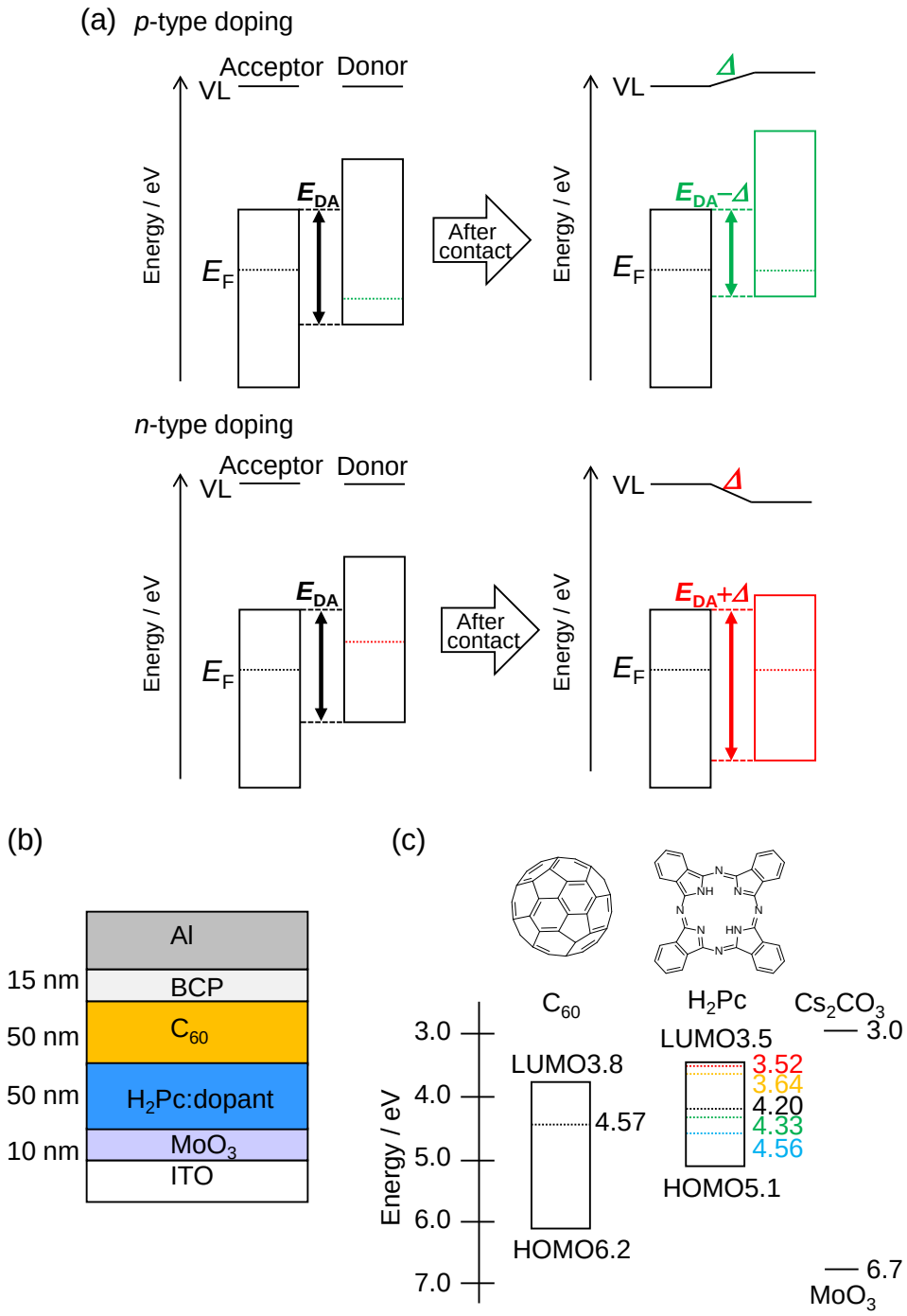

Fig. 4.3.1. (a) Schematic of E_F alignment at the D/A interface when the H_2Pc layer is doped with *p*-type and *n*-type dopants. (b) Schematic of the OSC device with a doped H_2Pc layer. (c) Chemical structures and energy levels of H_2Pc and C_{60}. The dashed lines indicate the W_F of nondoped (black), 200-ppm MoO_3 doped (green), 2,000-ppm MoO_3 doped (blue), 200-ppm Cs_2CO_3 doped (orange), and 2,000-ppm Cs_2CO_3 doped (red) H_2Pc layers (50 nm) on ITO substrates.

The *J–V* curves of the devices are shown in Fig. 4.3.2(a), and the device performances are summarized in Table 1. The PCE and V_{OC} of the nondoped device are 1.0% and 0.47 V, respectively; these values are very similar to those reported previously.[16] In the case of the PHJ devices with MoO_3-doped H_2Pc, the V_{OC} gradually decreased from 0.43 to 0.40 and 0.36 V for devices with dopant concentrations of 200, 2,000, and 20,000 ppm, respectively. These devices show similar fill factor (FF) values (~59%), indicating that charge recombination processes were not affected by the impurity doping. Therefore, the decrease in V_{OC} with increasing MoO_3 dopant concentration is attributed to the change in the W_F of the H_2Pc layer. In the case of the PHJ devices with Cs_2CO_3-doped H_2Pc, the V_{OC} increased from 0.47 V in the nondoped film to 0.51 and 0.52 V in films with dopant concentrations of 200 and 2,000 ppm, respectively. In contrast to the MoO_3 case, the J_{SC} and the FF steeply decreased with increasing Cs_2CO_3 concentration. The forward current in the dark condition decreased with increasing Cs_2CO_3 concentration, indicating that Cs_2CO_3 doping decreased the hole conductivity in the H_2Pc layer. Cs_2CO_3 doping caused a decrease of either the hole concentration or the hole mobility in the H_2Pc layer. Nevertheless, the V_{OC} change upon Cs_2CO_3 doping resulted in the opposite trend as the MoO_3 case; therefore, the author concluded that the W_F decrease in the H_2Pc film by Cs_2CO_3 doping was responsible for the V_{OC} increase. The W_F difference in the H_2Pc film induced by impurity doping resulted in V_{OC} values ranging from 0.36 V at an MoO_3 concentration of 20,000 ppm to 0.52 V at a Cs_2CO_3 concentration of 2,000 ppm (Fig. 4.3.2(b)). The large V_{OC} change of 0.16 V in total suggested that energy levels near the D/A interface were greatly shifted by the impurity doping.

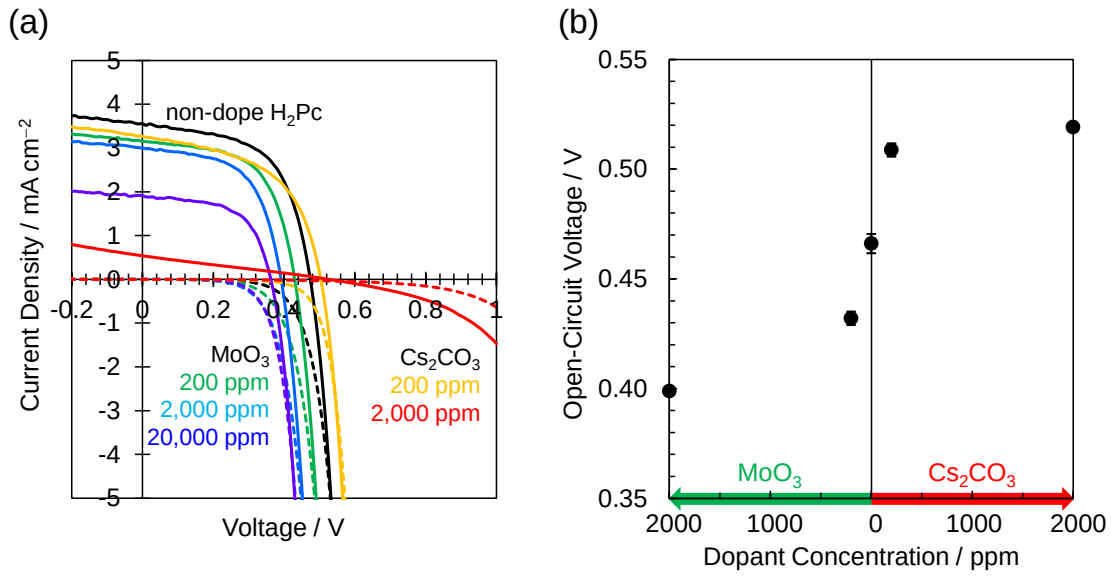

Fig. 4.3.2. (a) The *J*–*V* curves of non-doped H_2Pc/C_{60} devices (black) and the doped H_2Pc/C_{60} devices with MoO_3 concentrations of 200 ppm (green), 2,000 ppm (blue) and 20,000 ppm (purple) and Cs_2CO_3 concentrations of 200 ppm (yellow) and 2,000 ppm (red) under AM-1.5 irradiation (100 mW cm^{-2}, solid lines) or in the dark (dashed lines). (b) V_{OC} of doped H_2Pc/C_{60} devices as a function of dopant concentration.

Table 1. Summary of the performances of the doped H_2Pc/C_{60} devices with different concentrations of MoO_3 and Cs_2CO_3. Averaged values are reported.

Dopant	MoO_3			Nondoped	Cs_2CO_3	
Concentration / ppm	20,000	2,000	200	0	200	2,000
J_{SC} / mA cm^{-2}	1.91	3.05	3.30	3.68	3.37	0.53
V_{OC} / V	0.355	0.399	0.432	0.466	0.509	0.519
FF / %	58.6	59.1	59.6	58.8	53.8	25.5
PCE / %	0.40	0.72	0.85	1.01	0.92	0.07

4.3.2. Energy level mapping

To estimate the energy-level shift near the D/A interface, the author carried out energy-level mapping using the Kelvin probe method.[17,18] The W_Fs of C_{60} layers with different thicknesses were measured on ITO/Al/BCP substrates. Subsequently, the W_Fs of the H_2Pc layer with and without the dopants were measured on C_{60} layers.

The results of the energy-level mapping are shown in Fig. 4.3.3(a), along with the corresponding sample structure. The W_F of the C_{60} films on ITO/Al/BCP gradually increased from 3.12 eV at a film thickness of 0 nm to 4.18 eV at a film thickness of 50 nm. The W_F of non-doped H_2Pc films on C_{60} layers steeply increased from 4.18 eV at the surface of the C_{60} film to 3.88 eV at a H_2Pc film thickness of 10 nm and became constant as the thickness was increased further. The negative shift originated from the charge transfer induced by the E_F difference between the H_2Pc and C_{60} layers; this E_F difference formed a large electrostatic field near the D/A interface, which in turn led to the VL shift. The W_F of the film doped with 2,000 ppm MoO_3 shifted in the positive direction, showing a W_F of 4.18 eV at the surface of the C_{60} film to 4.55 eV at a doped H_2Pc film thickness of 50 nm because the E_F of the *p*-doped H_2Pc became deeper than that of the C_{60}. By contrast, the W_F of the H_2Pc film doped with 2,000 ppm Cs_2CO_3 showed a large negative W_F change from 4.18 eV at the surface of the C_{60} film to 3.54 eV at 50 nm. The large E_F difference between the Cs_2CO_3-doped H_2Pc layer and the C_{60} layer formed a large electrostatic field.

The energy diagrams based on the results of band mapping are shown in Fig. 4.3.3(b). The author assume that the positions of the HOMO and LUMO energy levels relative to the vacuum level are constant irrespective of the presence of dopant.[19,20] The VL shifted steeply within 10 nm near the D/A interface because of the charge

transfer, and the direction of the shift varied depending on the dopant. MoO_3 doping induced an energy-level shift that decreased the E_{DA}, whereas Cs_2CO_3 doping increased the E_{DA}. The direction of the E_{DA} change corresponded to the V_{OC} difference. However, the eV_{OC} difference of 0.16 eV is much smaller than the HOMO energy-level difference of 0.87 eV between MoO_3- and Cs_2CO_3-doped H_2Pc films 10 nm from the D/A interface. A recent report suggested that some portion of the generated charges formed by E_F alignment were transferred from the interface to the substrate; as a result, a weak electrostatic field was applied over the entire range of the film instead of near the interface.[21] The shift obtained by energy-level mapping might be overestimated. Another noteworthy point is that the energy-level shift was almost completed less than 10 nm from the D/A interface. Therefore, the doping effect near the interface might determine the device performance.

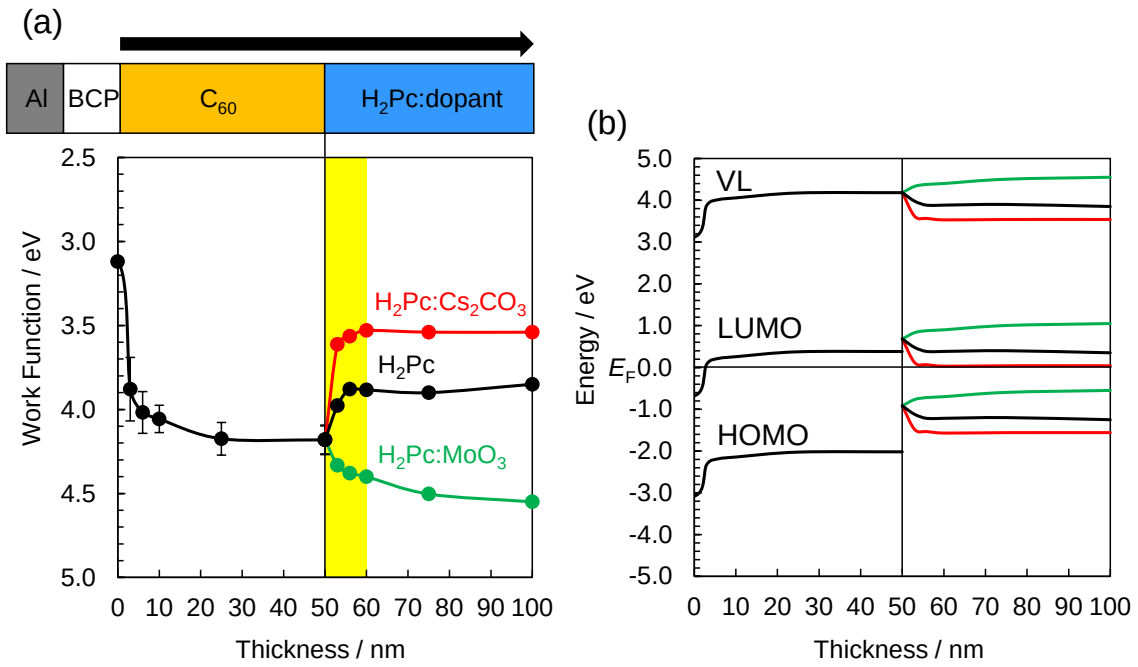

Fig. 4.3.3. (a) W_F of C_{60} films and H_2Pc films without dopant (black) and with 2,000 ppm of MoO_3 (green) and Cs_2CO_3 (red), as measured by the Kelvin probe method and plotted as a function of the thickness. The C_{60} and H_2Pc films were stacked on BCP/Al/ITO substrates; the corresponding sample structure is described at the top of the figure. The value of 0 nm corresponds to the W_F of the surface of the BCP/Al/ITO substrate. The region corresponding to a thickness less than 10 nm is highlighted. (b) Energy levels relative to the E_F of C_{60} films and H_2Pc films without dopant (black) and with 2,000 ppm of MoO_3 (green) and Cs_2CO_3 (red); these results are based on the results in Fig. 4.3.3(a). We assumed that the positions of the HOMO and the LUMO energy levels relative to the vacuum level are constant irrespective of the presence of dopant.

4.3.3. Device performance of the H_2Pc/doped H_2Pc/C_{60} device

To investigate the effect of impurity doping near the D/A interface, the author fabricated trilayer devices with a structure of ITO/MoO_3/H_2Pc/doped H_2Pc/C_{60}/BCP/Al. The H_2Pc/doped H_2Pc layers were stacked, with thicknesses of 45 nm/5 nm and 40 nm/10 nm. The thin doped H_2Pc layer constituted the D/A interface of the trilayer devices, and the nondoped H_2Pc layer existed apart from the D/A interface.

The *J*–*V* curves of the trilayer devices with a 2,000-ppm MoO_3-doped layer or a 2,000-ppm Cs_2CO_3-doped layer are shown in Fig. 4.3.4(a) and 4.3.4(b), respectively, and the device performances are summarized in **Table 2**. The device with a 5 nm MoO_3-doped layer showed a V_{OC} of 0.44 V, whereas the device with a 10 nm MoO_3-doped layer showed a decrease in the V_{OC} to 0.41 V, which was approximately the same value as the bilayer device with a 50 nm MoO_3-doped layer (0.40 V). The FF and J_{SC} of the trilayer devices with 5 nm and 10 nm MoO_3-doped layers were similar to those of the bilayer device with a 50 nm MoO_3-doped layer. Similar V_{OC} trends were observed for the devices with Cs_2CO_3-doped films. The device with a 5 nm Cs_2CO_3-doped layer showed a V_{OC} of 0.50 V, and the device with a 10 nm Cs_2CO_3-doped layer showed an increased V_{OC} of 0.52 V; these values are approximately the same as those of the bilayer device with a 50 nm Cs_2CO_3-doped layer (0.52 V).

These results indicate that 10 nm-thick doped layers determined the magnitude of the increase or decrease of the V_{OC}, consistent the band-mapping results (Figs. 4.3.3 and 4.3.4(c)). Notably, the device with a thinner Cs_2CO_3-doped layer showed larger J_{SC} and FF values. These results indicate that the origin of the decrease of the J_{SC} and FF in the devices with a Cs_2CO_3-doped layer was deterioration of the hole transport in the bulk and that this effect can be avoided by replacing the doped bulk layer with a

nondoped bulk layer. These results also indicate that doping only near the D/A interface could result in an increase in the V_{OC} while maintaining the J_{SC} and FF values.

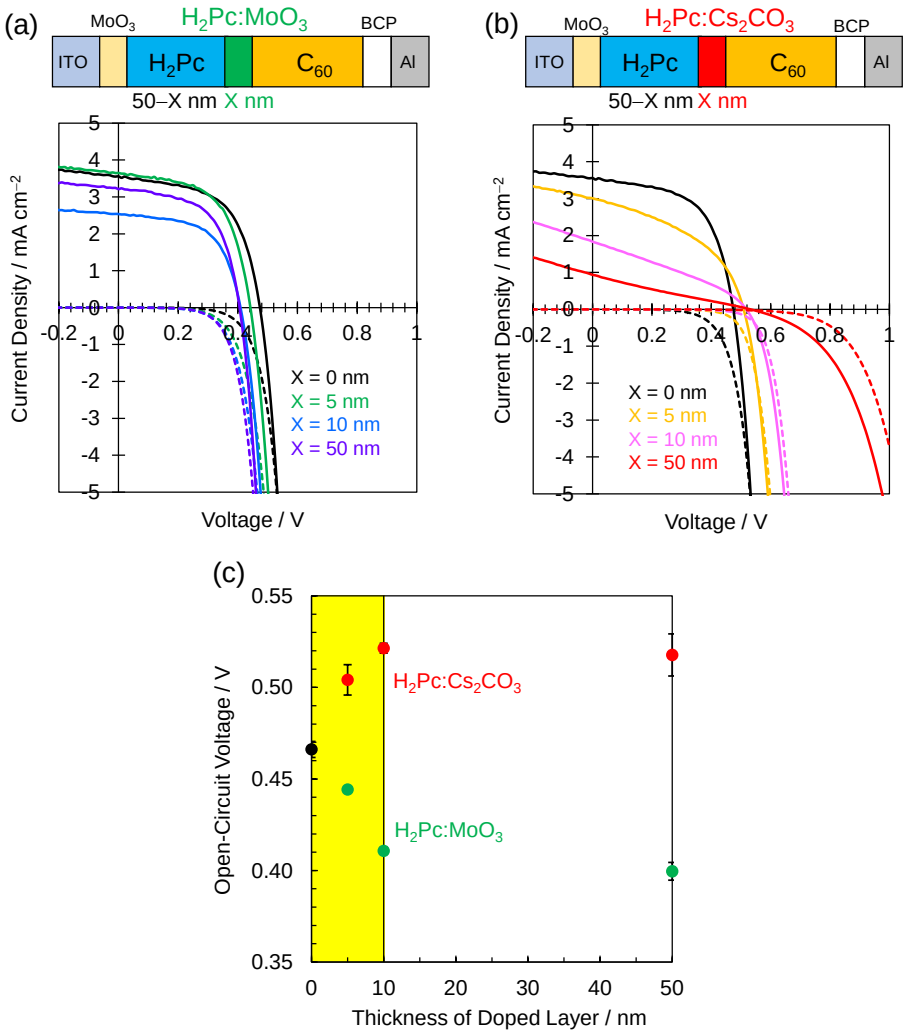

Fig. 4.3.4. Schematic of the structure of trilayer devices and the *J*–*V* curves of the devices with (a) 0 nm (black), 5 (green), 10 (blue), and 50 (purple) nm of 2,000-ppm MoO_3-doped H_2Pc layer and (b) 0 nm (black), 5 (yellow), 10 (pink), and 50 (red) nm of 2,000-ppm Cs_2CO_3-doped H_2Pc layer under AM-1.5 irradiation (100 mW cm^{-2}, solid lines) or in the dark (dashed lines). (c) V_{OC} of trilayer devices as a function of the thickness of the doped layers. The region corresponding to a thickness less than 10 nm is highlighted.

Table 2**.** Summary of the performances of the trilayer devices with different thicknesses of MoO_3- and Cs_2CO_3-doped H_2Pc layers. The table shows averaged values.

Dopant	MoO_3			Cs_2CO_3		
Thickness (nm)	5	10	50	5	10	50
J_{SC} (mA cm^{-2})	3.64	2.53	3.03	2.99	1.86	1.36
V_{OC} (V)	0.444	0.411	0.400	0.504	0.521	0.518
FF (%)	59.1	58.8	58.9	42.9	31.3	25.2
PCE (%)	0.96	0.61	0.71	0.65	0.30	0.19

4.4. Conclusions

In summary, the author demonstrated that impurity doping strongly affects the V_{OC} in PHJ devices. The addition of a *p*-type dopant in the donor layer decreased the V_{OC}, whereas the addition of an *n*-type dopant increased it. The wide range of V_{OC} change was explained by the large energy-level shift within 10 nm of the D/A interface as a result of E_F alignment between the donor and acceptor layers. The results demonstrated that the V_{OC} in organic solar cells are determined not only by the choice of the donor and acceptor materials but also by the energy-level shift near the D/A interface. The results also showed that the shift and the V_{OC} could be controlled through impurity doping. The next challenge is to control the energy-level shift near the D/A interface and the V_{OC} in BHJ devices via impurity doping. Such control could be realized through selectively introducing the dopant into the donor or acceptor phases in the blend films

4.5. References

[1] H.-Y. Chen, J. Hou, S. Zhang, Y. Liang, G. Yang, Y. Yang, L. Yu, Y. Wu, G. Li, Polymer solar cells with enhanced open-circuit voltage and efficiency, Nat. Photonics. 3 (2009) 649–653. doi:10.1038/nphoton.2009.192.

[2] L. Lu, T. Zheng, Q. Wu, A.M. Schneider, D. Zhao, L. Yu, Recent Advances in Bulk Heterojunction Polymer Solar Cells, Chem. Rev. 115 (2015) 12666–12731. doi:10.1021/acs.chemrev.5b00098.

[3] N.K. Elumalai, A. Uddin, Open circuit voltage of organic solar cells: an in-depth review, Energy Environ. Sci. 9 (2016) 391–410. doi:10.1039/C5EE02871J.

[4] M.C. Scharber, D. Mühlbacher, M. Koppe, P. Denk, C. Waldauf, A.J. Heeger, C.J. Brabec, Design rules for donors in bulk-heterojunction solar cells - Towards 10 % energy-conversion efficiency, Adv. Mater. 18 (2006) 789–794. doi:10.1002/adma.200501717.

[5] J.X. Tang, C.S. Lee, S.T. Lee, Electronic structures of organic/organic heterojunctions: From vacuum level alignment to Fermi level pinning, J. Appl. Phys. 101 (2007) 64504. doi:10.1063/1.2710297.

[6] S. Braun, W.R. Salaneck, M. Fahlman, Energy-Level Alignment at Organic/Metal and Organic/Organic Interfaces, Adv. Mater. 21 (2009) 1450–1472. doi:10.1002/adma.200802893.

[7] M. Oehzelt, K. Akaike, N. Koch, G. Heimel, Energy-level alignment at organic heterointerfaces, Sci. Adv. 1 (2015) e1501127–e1501127. doi:10.1126/sciadv.1501127.

[8] H.Y. Mao, F. Bussolotti, D.-C. Qi, R. Wang, S. Kera, N. Ueno, A.T.S. Wee, W. Chen, Mechanism of the Fermi level pinning at organic donor–acceptor

heterojunction interfaces, Org. Electron. 12 (2011) 534–540. doi:10.1016/j.orgel.2011.01.003.

[9] Y. Shinmura, M. Kubo, N. Ishiyama, T. Kaji, M. Hiramoto, pn- control and pn-homojunction formation of metal-free phthalocyanine by doping, AIP Adv. 2 (2012) 32145. doi:10.1063/1.4747814.

[10] Y. Shinmura, Y. Yamashina, T. Kaji, M. Hiramoto, Ionization sensitization of doping in co-deposited organic semiconductor films, Appl. Phys. Lett. 105 (2014) 183306. doi:10.1063/1.4901408.

[11] M. Hiramoto, M. Kubo, Y. Shinmura, N. Ishiyama, T. Kaji, K. Sakai, T. Ohno, M. Izaki, Bandgap Science for Organic Solar Cells, Electronics. 3 (2014) 351–380. doi:10.3390/electronics3020351.

[12] Y. Zhang, H. Zhou, J. Seifter, L. Ying, A. Mikhailovsky, A.J. Heeger, G.C. Bazan, T.-Q. Nguyen, Molecular Doping Enhances Photoconductivity in Polymer Bulk Heterojunction Solar Cells, Adv. Mater. 25 (2013) 7038–7044. doi:10.1002/adma.201302159.

[13] C. Ohashi, Y. Shinmura, M. Kubo, M. Hiramoto, Effects of doping at the ppm level in Simple n^+p-homojunction organic photovoltaic cells, Org. Electron. 27 (2015) 151–154. doi:10.1016/j.orgel.2015.09.001.

[14] Z. Shang, T. Heumueller, R. Prasanna, G.F. Burkhard, B.D. Naab, Z. Bao, M.D. McGehee, A. Salleo, Trade-Off between Trap Filling, Trap Creation, and Charge Recombination Results in Performance Increase at Ultralow Doping Levels in Bulk Heterojunction Solar Cells, Adv. Energy Mater. 6 (2016) 1601149. doi:10.1002/aenm.201601149.

[15] K. Nakano, K. Tajima, Organic Planar Heterojunctions: From Models for

Interfaces in Bulk Heterojunctions to High-Performance Solar Cells, Adv. Mater. 29 (2017) 1603269. doi:10.1002/adma.201603269.

[16] M. Kubo, Y. Shinmura, N. Ishiyama, T. Kaji, M. Hiramoto, Invertible organic photovoltaic cells with heavily doped organic/metal ohmic contacts, Appl. Phys. Express. 5 (2012) 92302. doi:10.1143/APEX.5.092302.

[17] H. Ishii, N. Hayashi, E. Ito, Y. Washizu, K. Sugi, Y. Kimura, M. Niwano, Y. Ouchi, K. Seki, Kelvin probe study of band bending at organic semiconductor/metal interfaces: examination of Fermi level alignment, Phys. Status Solidi. 201 (2004) 1075–1094. doi:10.1002/pssa.200404346.

[18] Y. Yamashina, Y. Shinmura, N. Ishiyama, T. Kaji, M. Hiramoto, Mapping of band-bending in organic pn-homojunctions, J. Appl. Phys. 117 (2015) 125501. doi:10.1063/1.4915506.

[19] S.D. Ha, J. Meyer, A. Kahn, Molecular-scale properties of MoO_3-doped pentacene, Phys. Rev. B. 82 (2010) 155434. doi:10.1103/PhysRevB.82.155434.

[20] M. Kröger, S. Hamwi, J. Meyer, T. Riedl, W. Kowalsky, A. Kahn, P-type doping of organic wide band gap materials by transition metal oxides: A case-study on Molybdenum trioxide, Org. Electron. 10 (2009) 932–938. doi:10.1016/j.orgel.2009.05.007.

[21] K. Akaike, N. Koch, M. Oehzelt, Fermi level pinning induced electrostatic fields and band bending at organic heterojunctions, Appl. Phys. Lett. 105 (2014) 223303. doi:10.1063/1.4903360.

Chapter 5:

General Conclusion

5.1. Summary of this thesis

This thesis can be summarized as follows.

1) The hole and electron ranges in the co-deposited films were estimated to be 0.34 and 9.4 μm, respectively, by impedance spectroscopy. The charge carrier ranges are far greater than the typical thickness of organic photovoltaic cells, indicating that, in the absence of charge carrier recombination, electrons and holes photogenerated in H_2Pc:C_{60} co-deposited films can be collected by their respective electrodes.

2) The reductions in V_{OC} due to bimolecular and the trap-assisted recombination in the H_2Pc/C_{60} devices were estimated to be 0.55 and 0.32 V, respectively. The temperature dependence of the reaction order revealed that charge trapped at localized states was the main cause of the fast recombination. If the number of localized states could be decreased, H_2Pc/C_{60} devices have the potential for larger V_{OC}.

3) The value of V_{OC} can be controlled by impurity doping. The energy band structure near the donor/acceptor interface has a major effect on the value of V_{OC}. *n*-type doping increased V_{OC} to 0.52 V in H_2Pc/C_{60} devices due to the increase in E_{DA} resulting from the vacuum level shift.

5.2. Future prospects

The author believes that the results in this thesis will lead to the following prospects

1) The hole and electron ranges in other active layer will be estimated. Furthermore, the range of the charge carriers will be a figure-of-merit for charge transport in organic semiconductor films.

2) Controlling V_{OC} by impurity doping will be applied to co-deposited films. Increased V_{OC} and high J_{SC} will lead to enhancements of the PCE.

List of Publications

All papers are included in this doctoral thesis.

1) Hole- and electron-only transport in ratio-controlled organic co-deposited films observed by impedance spectroscopy

   Naoto Shintaku, Seiichiro Izawa, Kenichiro Takagi, Hiroyoshi Naito, Masahiro Hiramoto

   Org. Electron., **50**, 515-520 (2017).

2) Effect of trap-assisted recombination on open-circuit voltage loss in phthalocyanine/fullerene solar cells

   Naoto Shintaku, Masahiro Hiramoto, Seiichiro Izawa

   Org. Electron., in press. DOI:10.1016/j.orgel.2018.01.016.

3) Controlling open-circuit voltage in organic solar cells by impurity doping

   Naoto Shintaku, Masahiro Hiramoto, Seiichiro Izawa

   J. Phys. Chem. C, revising according to reviewers' comments.

Poster Presentations in International Conferences

1) Determination of carrier range in C_{60}:H_2Pc co-deposition film used by impedance spectroscopy

   Naoto Shintaku, Chika Ohashi, Mitsuru Kikuchi, Kenichiro Takagi, Hiroyoshi Naito, Masahiro Hiramoto.

   The 3rd Workshop on Physics in Organic Optoelectronics,

   Institute for Molecular Science, Japan, 10th December 2015.

2) Determination of carrier range in C_{60}:H_2Pc co-deposition film used by impedance spectroscopy

   Naoto Shintaku, Chika Ohashi, Mitsuru Kikuchi, Kenichiro Takagi, Hiroyoshi Naito, Masahiro Hiramoto.

   The winter school of Asian CORE program—Molecular sciences for Energy, Environment, and Life,

   Institute of Chemistry Chinese Academy of Sciences (ICCAS), China, 28th February 2016.

3) Determination of carrier range in C_{60}:H_2Pc co-deposition films by impedance spectroscopy

   Naoto Shintaku, Chika Ohashi, Mitsuru Kikuchi, Kenichiro Takagi, Hiroyoshi Naito, Masahiro Hiramoto.

   Materials Research Society Singapore (IUMRS-ICEM2016),

   Suntec Singapore Convention & Exhibition Centre, Singapore, 6th June 2016

4) Determination of carrier range in C_{60}:H_2Pc co-deposited films using impedance spectroscopy

Naoto Shintaku, Kenichiro Takagi, Hiroyoshi Naito, Masahiro Hiramoto

Korea-Japan Joint Forum (KJF-ICOMEP 2016),

Acros Fukuoka, Japan, 5th September 2016

5) Hole- and Electron-only transport in ratio－controlled organic co－deposited films observed by impedance spectroscopy

Naoto Shintaku, Seiichiro Izawa, Kenichiro Takagi, Hiroyoshi Naito, Masahiro Hiramoto.

The 27th International Photovoltaic Science and Technology (PVSEC-27)

Lake Biwa Otsu Prince Hotel, Japan, 16th November 2017

Oral Presentations in Conferences (in Japanese)

1) The charge carrier mobility in C_{60} : H_2Pc co-deposited film measured by impedance spectroscopy.

   Naoto Shintaku, Chika Ohashi, Mitsuru Kikuchi, Kenichiro Takagi, Hiroyoshi Naito, Masahiro Hiramoto.

   The 76 th Japan Society of Applied Physics Autumn Meeting,

   Nagoya Congress Center, Aichi, 15th September 2015.

2) Evaluation of Recombination Processes in Organic Photovoltaics by Impedance Spectroscopy

   Naoto Shintaku, Seiichiro Izawa, Masahiro Hiramoto,

   The 64 th Japan Society of Applied Physics Spring meeting**,**

   Pacifico Yokohama, Kanagawa, 14th March 2017.

3) Photo-generated carrier transport mechanism of C_{60} : H_2Pc co-deposited films

   Naoto Shintaku, Seiichiro Izawa, Hiroyoshi Naito, Masahiro Hiramoto

   The 64 th Japan Society of Applied Physics Spring meeting**,**

   Pacifico Yokohama, Kanagawa, 15th March 2017.

4) Hole- and electron-only transport in ratio-controlled H_2Pc:C_{60} co-deposited films observed by impedance spectroscopy

   Naoto Shintaku, Seiichiro Izawa, Hiroyoshi Naito, Masahiro Hiramoto,

   The 78th Japan Society of Applied Physics Autumn meeting**,**

   Fukuoka Convention Center, Fukuoka, 5th September 2017.

5) The Effect of Impurity Doping on the Performance of Bilayer Organic Solar Cells.

Naoto Shintaku, Seiichiro Izawa, Masahiro Hiramoto.

The 78th Japan Society of Applied Physics Autumn meeting**,**

Fukuoka Convention Center, Fukuoka, 7th September 2017.

Poster Presentation in Conference (in Japanese)

1) Determination of carrier range in C_{60}:H_2Pc co-deposition film used by impedance spectroscopy

   Naoto Shintaku, Chika Ohashi, Mitsuru Kikuchi, Kenichiro Takagi, Hiroyoshi Naito, Masahiro Hiramoto

   Workshop on the current issue and future vision of organic solar cells development, Nara Institute of Science and Technology (NAIST), Nara, 28th November 2015.

Acknowledgements

This study has been conducted under the supervision of Prof. Masahiro Hiramoto. I am extremely grateful to Prof. Masahiro Hiramoto for providing me with the opportunity to study in his group. His scientific discussions and advice have always encouraged me.

I wish to thank Assis. Prof. Seiichiro Izawa. His comments and consideration have supported my research.

I would also like to thank Prof. Satoshi Kera, Assoc. Prof. Toshikazu Nakamura, Assoc. Prof. Toshiyasu Suzuki of IMS and Prof. Hiroyoshi Naito of Osaka Prefecture University, for their reviews of this thesis.

I'm thankful to the co-authors of the papers, particularly Dr. Kennichiro Takagi for his technical and theoretical advice. I'm also thankful to all the group members; Dr. Yusuke Shinmura, Dr. Masayuki Kubo, Dr. Chika Ohashi, Mr. Mitsuru Kikuchi, and Mr. Masaki Hirota each provided me with helpful comments on the experiments and the research.

I'm thankful to Ms. Hidemi Sugihara and Ms. Megumi Kobayashi for their support while carrying out my research.

I appreciate the financial support from the Okazaki Shinkin Bank through an Okashin Advanced Science Scholarship and the New Energy and Industrial Technology Development Organization (NEDO).

Finally, I would like to thank my parents and family for supporting and encouraging me and I am deeply grateful for their support and help during my time as a Ph.D. student.